THE MECHANISM OF BENEFICIAL EFFECTS

OF BORON AND ZIRCONIUM

ON CREEP=RUPTURE PROPERTIES OF A COMPLEX

HEAT=RESISTANT ALLOY

by

R. F. Decker

J. W. Freeman

Report 57

to

THE NATIONAL ADVISORY COMMITTEE FOR AERONAUTICS

October 11, 1957

Project 1478=11

ACKNOWLEDGMENTS

SUMMARY

A microstructural investigation was pursued to establish the
mechanism of the pronounced benefits of boron and zirconium on creep=
rupture properties of a 55 Ni - 20 Cr - 15 Co - 4 Mo - 3 Ti - 3 Al alloy
at 1600°F.

Materials with varying boron and zirconium content were exposed
to creep conditions and then the microstructures were analyzed by optical
and electron microscopy, electron diffraction, microfractography and
hardness measurements. Particularly useful were interrupted creep
tests which allowed comparisons of materials after equivalent creep
exposures.

The mechanism of improvement of creep-rupture properties was
found to be a pronounced stabilizing effect of boron and zirconium on the
grain boundaries of the alloy. The alloy with low boron and zirconium was
subject to rapid agglomeration of $M_{23}C_6$ and γ' in the grain boundaries, followed
by depletion of γ' and intergranular micro-cracking at the grain boundaries
transverse to applied stress. Brittle fracture then occurred by linking of
micro-cracks. However, additions of zirconium, boron and boron plus zircon-
ium decreased this tendency in that order. In the absence of these elements
extensive micro-cracking was found early in second-stage creep at relatively
short time periods and fracture occurred prematurely with very little deforma-
tion. Proper amounts of boron plus zirconium delayed micro-cracking until
after third=stage creep started so that creep-rupture life was greatly prolonged
and ductility to fracture markedly increased.

No effect of the trace elements on the size, amount and distribution of the
intragranular γ' was detected. Accordingly the property effects were not found
to result from a change in the intragranular γ' reaction.

The significant structural features were evident only after limited
amounts of creep. The damaging structural changes tend to be comparable at
fracture for material with varying amounts of trace elements even though there
are wide differences in rupture time and ductility when tested at a common stress.
An estimate of the generality and limitations of the mechanism is given in the
report.

INTRODUCTION

Recent investigations have revealed the importance of trace boron and zirconium in determining the creep-rupture properties of heat-resistant nickel-base alloys. This study is concerned with the mechanism of the effects.

Effects of Boron and Zirconium on Creep-Rupture Properties

A recent study (ref. 1) of effects of variable melting practice on heat-to-heat variations in properties of a 55 Ni - 20 Cr - 15 Co - 4 Mo - 3 Ti - 3 Al alloy indicated that introduction of trace boron or zirconium, inadvertently from crucible contamination or purposefully in "deoxidation," was the most important melting practice variable.

In summary, the findings were:

1. Creep-rupture life and ductility at 1600°F and 25,000 psi increased with boron content when zirconium was less than 0.01 percent (figs. 1 and 2).

2. Creep-rupture life and ductility at 1600°F and 25,000 psi increased with zirconium content when boron was less than 0.0005 percent (figs. 3 and 4).

3. The addition of 0.01 percent Zr to material containing 0.009 percent B raised both creep-rupture life and ductility significantly above the material with either element alone.

4. Minimum second-stage creep rates were lowered slightly by zirconium and more markedly by boron (fig. 5).

The work of Koffler, Pennington and Richmond (ref. 2) showed benefits to both creep-rupture life and ductility of M252, Udimet 500, Inco 700, Nimonic 90 and Waspaloy alloys from boron and zirconium addition. Confirmation of effects of boron on commercial nickel-base alloys was presented by Darmara (ref. 3) and Jones (ref. 4).

The effects, however, are not wholly restricted to the nickel-base alloys. Similar beneficiation of creep-rupture properties of other alloy systems has been established in the past.

The Objective

Since the helpful effects of boron and zirconium on creep-rupture properties are found in many alloy systems, establishing the mechanism for the effects would be desirable. Such a mechanistic approach should increase knowledge in theory of alloying and give a more basic understanding of alloy design to resist creep. In addition, this might also reveal the nature and cause of rupture in these materials.

Therefore, the objective was to establish the mechanism for the beneficial effects of boron and zirconium on the creep-rupture properties of a heat-resistant nickel-base alloy. The experimental procedure for detection of the mechanism was a study of the microstructures.

A 55 Ni - 20 Cr - 15 Co - 4 Mo - 3 Ti - 3 Al base composition was selected because the effects were established on this composition and because stock with established creep-rupture properties and chemistry was available.

Established Relations of Microstructure to Properties

It is generally accepted that the favorable high-temperature properties of the Ti + Al hardened nickel-base alloys result from the precipitation of the intermetallic γ' phase within the matrix of the alloy. The γ' phase has been shown to have a face-centered cubic structure similar to that of the Ni_3 Al phase of the nickel-aluminum system with a lattice parameter closely matched to that of the matrix of the alloys (refs. 5 and 6). Compositionally, the phase has been shown to dissolve titanium and is frequently referred to as Ni_3 (Al, Ti).

The creep resistance of these alloys has been attributed to the presence of γ' (refs. 5 and 7) and to the fact that γ' forms in fine dispersion within the matrix; however, attempts to relate the distribution of the γ' particles with the metallurgical properties have been only moderately successful to date. Frey, Freeman, and

White (ref. 8) and subsequently Brockway and Bigelow (ref. 9) found that dispersion of the γ' particles in Inconel-X alloy correlated with creep-rupture properties at 1200°F, which was low in the aging range for this alloy; however, no correlation was obtained for rupture tests at 1500°F, which was high in the aging range. Betteridge and Smith (ref. 10) studied the relations between structure and creep properties of several Nimonic alloys when tested high in the aging range. Highest creep-rupture properties were obtained with the greatest volume percent of γ'. Baillie (ref. 11) found that best creep resistance in Ni - Cr - Al - Ti alloys was obtained with the highest density of γ' particles as counted in electron micrographs.

Carbide reactions occur in the Ti + Al hardened nickel-base alloys and have been related to properties. Among the carbides identified are $M_{23}C_6$ (refs. 9, 12 and 13), M_6C (refs. 12 and 13), $Cr_7 C_3$ (ref. 14) and TiC (refs. 12 and 13). The occurrence of a type of carbide is dependent both on the alloy content and the temperature of treatment. In general, the carbide reactions in these alloys are poorly understood. Their probable importance in controlling properties was indicated by Betteridge and Franklin (ref. 14) who established the benefits on rupture life of obtaining a high-temperature precipitate of $Cr_7 C_3$ before creep exposure of Nimonic alloys.

Judging from the moderate success of previous work in relating the γ' and carbide reactions to properties, it was logical that the effect of trace elements on the alloy was by modification of these property-controlling reactions. Therefore, a microstructural study of the reactions was undertaken as described below.

EXPERIMENTAL PROCEDURES

The general procedure was to observe microstructural changes when materials with varying boron and zirconium content were subjected to thermal treatments involving temperature and stress. The experimental methods are described below.

Material

The experimental heats of the 55 Ni - 20 Cr - 15 Co - 4 Mo - 3 Ti - 3 Al alloy had been induction melted in the University of Michigan vacuum-melting furnace. The virgin melting stock was comprised of electrolytic nickel, electrolytic chromium, electrolytic cobalt, arc-melted molybdenum, Ti 55A titanium, 99.99 percent aluminum pig, electrolytic manganese, 99.9 percent silicon powder and spectrographically pure carbon. Boron was added to Heats V + B and V + B + Zr as NiB. The zirconium contained in Heats V + Zr and V + B + Zr was derived from reaction with zirconia crucibles used in melting. Heat V was melted in an alumina crucible while Heat V + B was melted in magnesia.

The 10-pound ingots had been processed as follows:

1. Homogenized 1 hour at 2300°F, air cooled.

2. Surface ground.

3. Rolled to 7/8-inch bar stock from 2150°F; 22 passes, each of about 7-percent reduction in area, were used with 10-minute reheats at 2150°F between passes.

Chemical analyses had been made on sections of the bar stock which originally were at the ingot center. In addition, material after creep exposure was checked for boron content. The results are listed in table I. Boron and zirconium were determined to be the significant heat-to-heat variables. The heats were coded to

indicate the relative boron and zirconium level: Heat V having low boron and zirconium, Heat V + Zr having relatively high zirconium, Heat V + B having relatively high boron and Heat V + B + Zr having significant content of both boron and zirconium. All the stock was homogenized 2 hours at 2150°F and air cooled prior to further experimentation.

Stress Aging and Stress-Rupture Testing

Treatments under stress were performed in stress-rupture units with strain measurements being made with an extensometer-mirror system with a sensitivity of 0.000005 inches per inch.

Solution-treated bar stock was machined to 0.250-inch test specimens with a 1-inch gage section. A uniform time period of 4 hours of preheating at test temperature in the stress-rupture units was used before stress application. The stress-aged samples were interrupted at the desired time by release of the load and immediate removal from the furnace.

Hardness

Diamond pyramid hardness (DPH) was measured with a 50-kilogram load. Three impressions were made on each sample, both diagonals of each impression being measured. Statistical analysis of testing variability established that in the range of 200 to 340 DPH a hardness difference of 7 DPH was significant while in the range of 340 to 400 DPH a hardness difference of 9 DPH was significant.

Metallography

Light Microscopy

Metallographic samples were mechanically polished through wet papers to 600 grit and then with the majority, on wet cloths with Linde A and Linde B powders. A few, as noted in the figures, were electropolished after 600 grit paper in a solution

of 10 parts of perchloric acid (70 percent) and 90 parts of glacial acetic acid at 30 volts with a current density of 2 amperes per square inch. Cyclic polishing of 5 seconds on and 5 seconds off was employed for a total period of electrolysis of 30 seconds.

The procedure and etchant developed by Bigelow, Amy and Brockway (ref. 15) was used to best reveal the precipitating phases at 100, 1000 and 2000 diameters. Etching was electrolytically at 6 volts and a current density of 0. 8 amperes per square inch for periods of 5 to 7 seconds, depending upon the sample condition. The etchant composition was 12 parts of phosphoric acid (85 percent), 47 parts of sulfuric acid (96 percent) and 41 parts of nitric acid (70 percent).

Electron Microscopy

Metallographic samples were mechanically polished through wet papers to 600 grit. Following this was electropolishing with the procedure described in the previous section on light microscopy.

Etching for the electron microstructures was accomplished with the etchant described under light microscopy using 6 volts and a current density of 0. 8 amperes per square inch for periods of 1 to 5 seconds.

After etching, collodion replicas of the metallic surface were made. These were shadowed with palladium to increase contrast and reveal surface contours; polystyrene latex spheres of approximately 3400 A in diameter were placed on the replicas prior to shadowing to indicate the angle and direction of shadowing and to provide an internal standard for measurement of magnification. The micrographs reproduced in this paper are copies of direct prints from the original negatives; consequently, the polystyrene spheres appear black and the "shadows" formed by the palladium appear white.

Counting Techniques

Depleted grain boundaries, micro-cracks, nodules and surface cracks were detected in this study. In order to make the trends and comparisons quantitative, counts were made of the number of each feature in the area traversed. In the case of depleted grain boundaries, micro-cracks and nodules, surveying was with an oil-immersion lens at 1000 diameters on mechanically polished and etched specimens. An area of 0.008 square inches was covered, this being comprised of eight strips, each 0.2 inch by 0.005 inch. In the case of interrupted creep tests, the strips were longitudinal to the specimen axis at the center of the specimen and at the minimum cross section. In ruptured samples, the strips were again longitudinal, starting in the grains at the fracture surface and progressing away from the fracture. A depleted grain boundary was counted when a clear, white strip of matrix free of γ' particles was clearly seen along a grain boundary. Micro-cracks were easily distinguishable by their blackness which was in complete contrast to all other intragranular and intergranular features of the samples. Early doubts about the identity were eliminated when electropolishing enlarged and accentuated these black voids and when fins on electron microscope replicas were found where these had filled the micro-cracks. Each distinct micro-crack was counted; 1 micron was selected as the minimum size counted since shorter micro-cracks were not distinguishable from carbide-matrix interfaces. Counting of nodules were arbitrarily limited to those above 5 microns in diameter.

Intergranular surface cracks were counted on mechanically-polished creep specimens by traversing longitudinal section surfaces at 500 diameters. This cracking was found to be quite uniform over the reduced section of the specimens. In the case of interrupted creep specimens, the cracks were counted over the center 0.75 inches, while in ruptured samples, counts were made for 0.50 inches from the

fracture. Intergranular cracks penetrating more than 0.003 inches deep were counted.

A rough measure of γ' dispersion was obtained by the surface density of γ' particles in electron microstructures. An area large enough to contain at least 100 particles was surveyed at 12,000 diameters.

The above techniques allow quantitative comparison of the tendency of the four heats to undergo the changes. It is recognized that percent of grain boundary area cracked, percent of grain boundary area depleted, volume percent of nodules, and volume percent and interparticle distance of γ' would be fundamentally more sound quantities for correlation. However, these more refined and time-consuming techniques would not alter the conclusions of this paper and, therefore, were not considered necessary.

Electron Diffraction

The extraction-replica technique of Fisher (ref. 16) was used to permit identification of precipitating phases by electron diffraction.

Specimen Preparation

For extraction of intragranular γ', the specimen preparation was identical to the electropolishing and etching used for electron microscopy.

The specimen preparation for extraction of intragranular carbides consisted of electropolishing and then electrolytically etching for 15 minutes in 2 parts phosphoric acid (85 percent) to 8 parts water in order to remove γ'.

For extraction of intergranular particles, the microfractographic techniques of Plateau, Henry and Crussard (ref. 17) proved very useful. Specimens were cooled in liquid nitrogen and then fractured using a hammer and chisel, the fracture being intercrystalline. The fracture surface was then etched with the same procedure described above for electron microscopy.

Replication

Carbon replica films were deposited on the prepared surfaces by the method of Bradley (ref. 18) and were backed by thicker supporting films of collodion. The surfaces were then etched electrolytically in a solution of 2 parts phosphoric acid (85 percent) to 8 parts water until the compound replica films separated from them. The films were transferred to the surface of clean distilled water and allowed to wash by diffusion, picked up on nickel screens, washed again, and the collodion backing films dissolved from the carbon films with amyl acetate by the method of Jaffe (ref. 19). The replicas were then shadowed with aluminum to provide an internal standard for interplanar distances. Electron micrographs were obtained from the replicas in an RCA Model EML electron microscope. In addition, electron diffraction patterns were obtained from the particles by selected area electron diffraction techniques on the microscope.

Thermal Exposures Used Before Microstructural Examination

The four experimental heats were exposed to several treatments before microstructural examination. The exposures, purpose of each and limitations on comparison were:

1. No exposure initial condition as solution treated 2 hours at 2150°F, air cooled - to detect differences in microstructure before creep exposure.

2. Aged 1/2, 1, 4, 10, 100, 188 and 500 hours at 1600°F - to show response of materials to temperature effects alone.

3. Stress-aged 165 hours at 1600°F and 20,000 psi - to show response to creep exposures of equal stress and time (because of differing creep rates, as shown in figure 6, the total creep deformations were unequal).

4. Stress-aged to rupture at 1600°F and 25,000 psi - to show response to creep exposures of equal stress (because of varying rupture life and ductility as shown in figure 7, the exposure times and total creep deformations were unequal).

5. Stress-aged at 1600°F at stresses selected to give comparable time-elongation curves - to compare response to creep exposures of equal strain, strain rate and time (because of varying creep rates, the stresses were unequal as listed: Heat V - 20,000 psi, Heat V + Zr - 22,500 psi, Heat V + B - 28,000 psi, Heat V + B + Zr - 30,000 psi).

Rupture times for those stress-aged samples which were run to rupture are plotted in figure 8. Data on stress aging are listed in table II.

RESULTS

Marked microstructural changes occurred in Heat V during creep exposure at 1600°F. In terms of properties, the most significant changes were at the grain boundaries where a process of agglomeration of $M_{23}C_6$, depletion of γ' precipitates, micro-cracking and, finally, brittle fracture occurred. This process was retarded by zirconium, more by boron and most by boron with zirconium.

Other microstructural features developed during exposure at 1600°F, including intragranular M_6C in the heats with boron, alignment of γ', intergranular surface cracking and nodular mixtures of carbides and γ'. The details of the grain boundary changes as well as other microstructural changes are given in the following sections.

The light micrographs presented are mounted with the rolling direction (and axis of tension in the case of creep specimens) vertical and in the plane of the figure. The orientation of electron micrographs was not determined except where noted in the figures.

Microstructures in Initial Condition

After the initial homogenizing treatment of 2 hours at 2150°F and air cooling, the experimental heats were similar in grain size (fig. 9), inclusion count and distribution (fig. 9), and grain boundary precipitate (figs. 10 and 11). γ' precipitated during the air cooling after the 2150°F treatment. Some slight differences in dispersion of intragranular γ' existed but these were not found to be significant as discussed later. Hardnesses (fig. 9) did not differ significantly in this condition.

Changes in Microstructure During Exposure at 1600°F

Tables III and IV list the quantitative data on microstructural changes.

Agglomeration in Grain Boundaries

A network of carbides enveloped by γ' accumulated in the grain boundaries of all samples during exposure at 1600°F. In Heat V, the rate of accumulation was comparatively rapid, the carbide phase being extensive and blocky and the γ' layer thick after 165 hours exposure with 1.2 percent creep deformation (figs. 12, 13 and 14). The amount of agglomeration under these conditions was somewhat lower in Heat V + Zr and much lower in Heats V + B and V + B + Zr (figs. 13 and 14).

The agglomerated γ' was easily identified by etching characteristics. The agglomerate reacted to etching in the same manner as the intragranular γ' in all the experimental work carried out. It always was in the same relief and had the same appearance as the intragranular γ'.

Microfractographic techniques were used to identify the carbide phase and obtain more information on its form. Samples from Heats V and V + B after 1.2 percent creep deformation at 1600°F in 165 to 188 hours were cooled in liquid

nitrogen and then fractured. Extraction replication from the fractured surface removed the grain boundary carbide and retained it in the replica. Electron micrographs showing the size and distribution of carbides in the grain boundaries are shown in figure 15. The extracted particles from Heat V were larger, more extensive and thicker than those from Heat V + B. The electron diffraction spots obtained on the replicas of the two samples indexed for $M_{23}C_6$.

Depletion of γ' at Grain Boundary

Subsequent to the agglomeration of $M_{23}C_6$ in the grain boundaries, strips of matrix were depleted of γ' particles along transverse grain boundaries of the stress-aged specimens (fig. 16). This occurred most often adjacent to $M_{23}C_6$ particles. This was in contrast to samples aged without stress, where the intergranular $M_{23}C_6$ was always enveloped by γ' and where the fine γ' particles extended up to the grain boundary (figs. 17 and 18).

In figure 16, the amount of this depletion is related to creep deformation for the experimental heats exposed to give equal strain at equal time at 1600°F. It is evident that boron and zirconium are effective in reducing the amount of this depletion with a given strain at 1600°F. Since the samples were stressed to give comparable strain rates, it follows that depletion in a given time at 1600°F was reduced. Despite this retarding influence, however, the amounts of depletion at fracture became comparable under influence of increased strain in Heats V + Zr, V + B, and V + B + Zr.

In samples ruptured at 1600°F and 25,000 psi (fig. 19) the depletion was extensive. Often, layers of precipitate-free matrix as thick as 5 to 10 microns were found. In this case, comparison of retardation was limited by the unequal exposure times and strains.

After 165 hours at 1600°F at an equal stress of 20,000 psi, the retarding effect of boron and zirconium was even more evident. While 264 depleted boundaries were found in Heat V, only 72 were found in Heat V + Zr, 16 in Heat V + B and none in Heat V + B + Zr (table III).

Micro-cracks

Following agglomeration of $M_{23}C_6$ and depletion of γ' in the grain boundaries, micro-cracks appeared. These appeared as dark areas in mechanically polished samples (fig. 13). Confirming evidence of these was found in electron microscopy where the replicas contained fins where the collodion had filled micro-cracks and then had been extracted during stripping of the replica from the metal surface. The fins appeared black in the electron microstructures (fig. 14) with white shadows from palladium.

The micro-cracks were associated with $M_{23}C_6$ particles in the grain boundaries transverse or nearly transverse to the applied stress, usually being at an $M_{23}C_6$ - matrix interface or between tips of $M_{23}C_6$ particles, in both cases where depletion of γ' had occurred. Often, several separate micro-cracks were detected in one grain boundary with no preference being shown for triple points. These separate cracks seemed to link together with further creep exposure; this constituting the mode of fracture in Heat V.

Figure 20 relates micro-cracking to creep deformation for the experimental heats exposed to give equal strain in equal time at 1600°F. The number of cracks for a given creep strain or exposure time diminished in Heat V + Zr, Heat V + B and Heat V + B + Zr in that order. Five micro-cracks were dectected in Heat V at the end of first stage creep when only 15 percent of the rupture life was expended. In Heat V + B + Zr, only 2 micro-cracks were found at 80 percent of the rupture life when tertiary creep had already commenced. The amount of micro-cracking

at fracture also diminished in the order Heat V, Heat V + Zr, Heat V + B and Heat V + B + Zr. When the four heats were exposed 165 hours at 1600°F and 20,000 psi, the difference in micro-cracking was even more pronounced. 314 micro-cracks were counted in Heat V, only 9 in Heat V + Zr and none in Heats V + B and V + B + Zr.

It was evident from the specimens tested at 1600°F and 25,000 psi that, although micro-cracking was retarded, it was not prevented by boron and zirconium (table III).

Intergranular Surface Cracking

In addition to micro-cracks within the specimens, the heats were subject to intergranular cracking from the specimen surface during creep-rupture tests. Initiation of these cracks was definitely from the specimen surface with a gradual increase in number and depth during creep exposure. Some of these cracks are pictured in figure 21 with quantitative data on amounts listed. Figure 21 shows that the specimen of Heat V run at 1600°F and 25,000 psi had negligible surface cracking at the time of rupture, 52 hours. The mode of fracture was by linking of the interior micro-cracks evident in figure 21. However, in Heat V + B run at 1600°F and 28,000 psi, the amount of micro-cracking was diminished but surface cracking is evident (fig. 21). The importance of these surface cracks in fracture is indicated by the sample from Heat V + B + Zr run at 1600°F and 30,000 psi, where some of the surface cracks penetrated more than 1/4 of the specimen radius (fig. 21).

The quantitative data for surface cracks seems to indicate that the trace-element additions modified mode of fracture. Surface cracking increasingly competes with micro-cracking as a source of fracture when the tendency for micro-cracking is reduced.

Intragranular Precipitation of Carbide

In addition to decreased tendency for intergranular $M_{23}C_6$, a carbide precipitated intragranularly during exposure at 1600°F in the heats with boron more than in other heats (fig. 14).

The form of this phase was stress dependent. Short plate-like carbides formed in samples aged without stress. In the stress-aged samples these were more elongated in form (compare figs. 13 and 17) and had a tendency to precipitate on preferred matrix planes. As shown in figure 15, the phase was extracted from Heat V + B after 1.2 percent creep strain in 188 hours at 1600°F. The majority of spots in the electron diffraction pattern indexed for M_6C with some spots corresponding to $M_{23}C_6$. Therefore, it seemed that some of the intragranular carbide phase, if not all, was M_6C rather than $M_{23}C_6$.

The intragranular carbide was distributed fairly uniformly throughout the grains in the boron heats with some concentration near the Ti (C, N) particles.

There was some evidence that intragranular carbides diminished and carbides increased in the grain boundaries during long time exposure indicating that carbon was diffusing to the grain boundaries.

Intragranular γ'

The intragranular precipitates of γ' grew and agglomerated during aging at 1600°F. As measured by the surface density of γ' particles in electron micrographs there was no significant effect of boron, zirconium or stress on this reaction (fig. 22). Therefore, the differences in surface density of γ' existing after the 2150°F treatment and air cooling were not lasting and appeared to be unimportant.

As a further means of evaluating effects of trace elements on aging of γ' at 1600°F, the change of hardness with aging time at 1600°F was measured (fig. 23 and table IV). The hardness changes for the four experimental heats were very similar except that Heat V + B + Zr aged to a higher hardness and retained this advantage at 500 hours. All heats reached maximum hardness at 1600°F at about 1 hour and then overaged at longer times. Electron micrographs typical of the alloy showing γ' density are included in figure 23.

Although creep strain did not affect the density of γ' particles, it did modify the distribution of particles. Creep strains within the grains resulted in some preferential agglomeration of γ' on the slip planes, as evidenced by an alignment of γ'. This was especially noticeable after high creep strain (fig. 18).

Identification of the γ' phase was made by electron diffraction (fig. 15).

Nodular Precipitate

All the materials exhibited "nodules" to some extent after aging at 1600°F (fig. 23 and tables III and IV). The nodules, which often were seen to envelope or abut on carbon-rich Ti (C, N), appeared to be mixed carbide and γ'.

As shown in figure 23, their occurrence was definitely strain accelerated, especially in Heat V. Likewise, they were trace element controlled in that their formation was retarded by boron and zirconium.

Check of Boron Content after Creep Exposure

A specimen from Heat V + B was analyzed for boron content after rupture in 428 hours at 1600°F and 25,000 psi. The cross section of the specimen was analyzed at 0.0090 percent boron. A surface layer of approximately 0.010 inches depth contained 0.0079 percent boron. These compared with the analysis of 0.0089 percent boron obtained in the as-rolled bar stock.

DISCUSSION

The microstructural studies revealed the role of boron and zirconium in increasing creep-rupture life and ductility of the 55 Ni - 20 Cr - 15 Co - 4 Mo - 3 Ti - 3 Al alloy.

In the absence of boron and zirconium, $M_{23}C_6$ and γ' rapidly formed a network in the grain boundaries of the alloy during creep at 1600°F. This was followed by depletion of γ' precipitates in the metal adjacent to the transverse grain boundaries and early intergranular micro-cracking at the $M_{23}C_6$ - depleted zone interfaces. The micro-cracks grew, linked and initialed brittle and premature failure.

The role of boron and zirconium was to retard this grain boundary process, thereby allowing longer creep exposure and higher creep deformation before the fracture mechanism operated.

Additional experimental support for the mechanism is obtained by relating creep-rupture life (fig. 25) and ductility (fig. 26) at 1600°F and 25,000 psi to the tendency of the experimental heats to undergo depletion of grain boundaries and micro-cracking during 1.2 percent creep deformation in 165 to 214 hours at 1600°F.

It is evident from the data that the increase in creep-rupture life and ductility from the trace-element addition results from retardation, but not prevention, of the grain boundary mechanism of carbide formation, grain boundary depletion and micro-cracking. The specimens from all the experimental heats were similar in degree of grain boundary agglomeration of carbides, γ' depletion and micro-cracking after rupture at 1600°F and 25,000 psi. However, both the time and deformation at which the grain boundary effects occurred and initiated fracture were increased by boron and zirconium.

The finding of only retardation of micro-cracking by boron and zirconium does not imply that their beneficial effects are only temporary in nickel-base alloys. All available data indicate that the boron and zirconium materials are superior to those free of boron and zirconium even at low stresses and in long-time exposure.

The chemical analyses on Heat V + B after rupture testing indicated that loss of boron from the sample during testing did not occur except possibly at the surface. De-boronization does not appear to be the cause of the eventual appearance of the grain boundary changes in boron-bearing material.

Interpretation of Other Microstructural Changes

There are several other features of the data which require discussion.

Intragranular Carbide Precipitation

Apparently the occurrence of intragranular carbide in the heats with boron was related to retardation of $M_{23}C_6$ agglomeration in the grain boundaries. In a sense, a redistribution of carbide was affected by boron. In the case of zirconium additions, suppression of the grain boundary agglomeration was not accompanied by intragranular carbides, possibly because of the weaker effect at the grain boundary.

The intragranular carbide in the boron heats may have had a direct effect on properties in addition to tying up carbon to retard $M_{23}C_6$ agglomeration in grain boundaries. The form of the precipitate after creep indicates that it is strain-induced and may lower creep rate in a manner proposed by Cottrell (ref. 20). According to Cottrell, resistance to creep is obtained by nucleation and growth of precipitates in dislocations, preventing further movement of the dislocations through the lattice. The reaction would resemble strain aging, although the resulting precipitate would be more advanced in growth than that usually associated with strain aging.

The negative creep and slight serrated effect in the creep curves of the boron heats at 1600°F and 20,000 psi appear to be additional evidence of strain-induced precipitation. These phenomena have been observed in other nickel-base alloys containing boron in unpublished work in this laboratory.

The presence of strain-aging type reactions in nickel-base alloys is not totally unexpected in that Wache (ref. 21) has detected serrated stress-strain curves for 80 Ni - 20 Cr alloys up to 1292°F.

Although the above evidence indicates that strain-induced carbide precipitate might have lowered creep rate, the proof was not considered positive.

Depletion

The depletion of γ' definitely required stress. No evidence of its occurrence was observed in any case when exposed to 1600°F without stress. It was furthermore more prevalent in the transverse grain boundaries. The absence of γ' depletion when the alloy was aged at 1600°F without stress indicates that the reaction was not due to simple depletion of elements forming γ' from the adjoining matrix by the grain boundary precipitates. It seems probable that the depletion mechanism was strain-induced γ' agglomeration resulting from localized strain concentration at the grain boundaries.

Surface Cracking

The information obtained on the role of surface cracking was not sufficiently extensive to be sure of its role. The indications were that when boron or zirconium retarded micro-cracking to allow longer creep exposures or more highly stressed creep exposures, fracture was at least in part initiated by surface cracks.

Intragranular γ' Stability

It was initially thought that boron and zirconium might operate through some influence on the size, distribution or stability of the intragranular γ' reaction.

Since Baillie (ref. 11) succeeded in correlating creep-rupture properties with the surface density of γ' particles as measured in electron micrographs, surface density was used to detect possible effects of boron and zirconium on the γ' which would increase rupture life. No significant effect was found. In fact, these elements had so little effect on any aspect of γ' (other than in suppressing agglomeration and depletion of γ' at grain boundaries) that it seems certain that the boron-zirconium effect did not operate through the reaction.

In the absence of any observable effect on the γ', the reason for the higher hardness of Heat V + B + Zr is uncertain. It was noted that the hardness values were in the same order as the total Ti + Al in the heats. The slightly higher Ti + Al may account for the higher hardness of Heat V + B + Zr.

The distribution of the γ' after creep exposure was found to be a good indicator of the mode and location of creep deformation. Alignment of γ' seemed to indicate that creep deformation had been accommodated by the grains as coarse slip. This alignment had previously been found by Buckle and Poulignier to indicate the mode of deformation in nickel-base alloys (ref. 22).

Nodular Precipitate

The role of the nodules of mixed carbide and γ' was not clear. No evidence was found to indicate that cracking was initiated by its presence. It is possible that it contributed to the depletion of γ' adjacent to the grain boundaries by acting as a final location for the γ'. This hypothesis is somewhat supported by the accelerating effect of stress on nodular formation at 1600°F, particularly when γ' depletion occurred.

Relation of Mechanism to Published Information

The accumulation of $M_{23}C_6$ in grain boundaries has striking parallels to sensitization of stainless steels. Simpkinson (ref. 23) and Bungardt and Lennartz (ref. 24) have identified $Cr_{23}C_6$ as the grain boundary phase leading to stress corrosion of 18-8 stainless steels. In addition, Plateau, Henry and Crussard (ref. 17) found the size, shape and distribution of $Cr_{23}C_6$ in 18-8 stainless steels to be similar to that of $M_{23}C_6$ found in this study.

The agglomeration at grain boundaries during creep of Ti + Al hardened nickel-base alloys has been noted by Baillie and Poulignier (ref. 25) and Mathieu (ref. 26). Mathieu hypothesized that the precipitate was γ' and chromium compounds. Although it was stated that this agglomeration was probably important in determining rupture life, further details on the mechanism were not given.

The γ' and $M_{23}C_6$ network could influence properties in two ways. The $M_{23}C_6$ particles could act as heterogeneous nuclei for micro-cracks, lowering the requirements for micro-cracking. Also a continuous film in the grain boundaries can lead to stress concentrations at the grain boundaries. Strain on the slip planes running up to the grain boundary from one grain cannot pass into the adjoining grain because of blocking by the film (ref. 27). Thus, the opportunity for stress relief is reduced.

In accordance with the theories of Chang and Grant (ref. 27), depletion of precipitates in layers of matrix adjacent to grain boundaries would promote micro-cracking and fracture by concentrating deformation at these weak grain boundaries. It is possible that this mechanism operates in many high-temperature alloys to give brittle fractures when the creep resistance of the material remains high. Such an explanation was offered by Wever and Schrader (ref. 28) for brittle fracture of Cr - Ni - M_O steels in long-time service at

500°C. Localized precipitation of Mo_2C left a condition of strong grains and depleted grain boundaries. Further confirmation is obtained from work on the effect of cellular precipitation (refs. 29 and 30) where this left depleted regions in the grain boundaries and led to premature and brittle creep-rupture.

The location of micro-cracks at the $M_{23}C_6$ - matrix interface was interesting in light of the work of Resnick and Seigle (ref. 31), who established that ZnO particles were heterogeneous nuclei for micro-cracks in α-brass. As shown by Machlin (ref. 32), particle - matrix bonding is important in nucleation of micro-cracks. In general, the presence of second-phase particles makes nucleation more probable, especially when bonding is poor. Considering these effects, it seems probable that the $M_{23}C_6$ particles acted as nuclei for micro-cracks; possibly because of poor bonding.

The mechanism of nucleation and growth of micro-cracks is not clear. Several authors (refs. 31, 32, 33, 34, 35) have proposed condensation of vacancies formed during creep by dislocation movements. Others (refs. 27, 36, 37) emphasized local stress concentrations as the cause. Grain boundary sliding is usually considered to set up the local stress concentrations at the transverse boundaries to cause loss of cohesion. Chang and Grant (ref. 27) hypothesize that rate of growth of micro-cracks in grain boundaries depends upon the stress pattern at the boundaries. Propagation of micro-cracking is caused primarily by the normal stress at the grain boundary and the inability of the material to relieve this stress. The overall rate of growth depends upon the ability of the grains to accommodate the normal stresses by deformation within the grain. From this it can be inferred that micro-cracking increases as the severity of localization of deformation at grain boundaries increases. Therefore, change of the mode of deformation from intragranular slip to grain boundary creep can be

expected to increase grain boundary micro-cracking by redistribution of stresses. In fact, in α-brass the occurrence of micro-cracking is coincident with the change from coarse slip to grain boundary sliding (ref. 33). The evidence of increased intragranular slip and decreased micro-cracking in the boron and zirconium heats is in full agreement with the above theories. It appears feasible that the elements have changed the mode of deformation by maintaining the grain boundary strength.

The discrepancies of the literature on the time of micro-crack nucleation are not surprising, considering the effect of trace elements in this study. While several instances have been found of micro-cracking early in second-stage creep (refs. 34, 38, 39), other cases exist where none was found until tertiary creep (refs. 33, 40, 41). In this study, the case exists where, in one alloy, nucleation of micro-cracks can be delayed from early in second stage to early in third stage creep by trace elements.

Regarding the effect of micro-cracks on properties, the Russian theorists (refs. 35, 39, 42) attribute tertiary creep and rupture to a gradual destruction of the metal by micro-cracking. This implies that micro-cracking raises creep rate and lowers life and ductility. In addition, the normal break in the stress-rupture curve of commercial alloys associated with a change from transgranular to intergranular fracture is an important consideration. This change in fracture mechanism, which is essentially an increase in intergranular micro-cracking, results in lower life and ductility than predicted from higher stress data where micro-cracking was less predominant.

In general, the literature supports the mechanism established. The grain boundary process would be expected to raise creep rate and lower rupture life and ductility. It follows that retardation of the grain boundary changes by boron and zirconium would be the mechanism for the beneficial effects on properties.

Causes of Effect of Boron and Zirconium on Grain Boundary Stability

The experimental evidence established that trace amounts of boron and zirconium retard agglomeration at grain boundaries and thereby retard the micro-cracking mechanism. Several causes of this retardation of agglomeration might be proposed.

It can be hypothesized that boron and zirconium stabilize carbon directly in a less deliterious form than intergranular $M_{23}C_6$ in the same manner that titanium stabilizes carbon as Ti C in 18-8 stainless steels. One would expect to find evidence of boron-carbon or zirconium-carbon compounds in this case. Since none were detected, support for this theory is lacking.

A similar possibility would be that the elements are promoting stabilization of carbon indirectly by promoting the nucleation and growth of one carbide at the expense of another. This might result from solid solution of boron or zirconium in the complex carbides of the M_6C or $M_{23}C_6$ type. Indeed, the detection of intragranular carbides, apparently of the M_6C type, when boron was present is compatible with this hypothesis. However, lack of promotion of additional carbides by zirconium additions does not support this hypothesis.

An alternative reason might be found in equilibrium segregation. Cahn (ref. 43) has reviewed the relationships of grain boundaries to impurity distribution. When elements of odd atomic size exist in alloys, they are subject to inhomogeneous distribution. Because they do not fit well in the crystal lattice where high regularity exists, the odd-sized atoms segregate to regions of lower regularity where larger vacancies exist. Grain boundaries are a prime region of concentration because of their inherent irregularity. Experimental confirmation for this was obtained by Thomas and Chalmers (ref. 44) who found that polonium segregates to grain boundaries in Pb - Bi alloys.

The segregating tendencies of two competing odd-sized elements can be related to their degree of misfit in that the most odd-sized atoms will seek out the grain boundary more rapidly. Thus, small amounts of one very odd-sized element can be utilized to heal the grain boundary, thereby retarding the segregation of a less odd-sized element by decreasing the available holes in the grain boundary. The possibility exists that boron and zirconium are retarding carbon segregation by this mechanism.

Study of the atomic diameters of carbon, boron and zirconium might reveal the feasibility of this. Speiser, Spretnak and Taylor (ref. 45) have shown that the effective diameter of carbon in γ-Fe is 1.36 $\overset{\bullet}{A}$, while they postulate that boron has an effective diameter equivalent to or greater than 1.85 - 1.90 $\overset{\bullet}{A}$. Goldschmidt's metallic diameter (for coordination number of 12) for zirconium is 3.20 $\overset{\bullet}{A}$. The available lattice spaces in the 55 Ni - 20 Cr - 15 Co - 4 Mo - 3 Ti - 3 Al alloy can be calculated from the lattice parameter of 3.58 $\overset{\bullet}{A}$ established in unpublished work at this laboratory. The vacant interstitial space in solid solution is 1.05 $\overset{\bullet}{A}$ in diameter. Using the data on atomic diameters, the carbon atom is 29 percent larger, boron is 78 percent larger and zirconium is 200 percent larger than the available space. In the case of substitutional solution, the boron atom is 26 percent smaller, and zirconium 27 percent larger than the substitutional space of 2.52 $\overset{\bullet}{A}$ diameter. Therefore, it appears that carbon fits moderately well interstitially but that boron and zirconium fit poorly both as interstitials and in substitution. Then it seems feasible that boron and zirconium are segregating preferentially to grain boundaries, healing them and retarding carbon segregation.

Other aspects of the data lend support to the theory of equilibrium segregation. Decreased tendency for γ' agglomeration at the grain boundaries in the boron and zirconium heats could result from the boron and zirconium healing the grain boundaries. The promotion of intragranular carbide by boron might be the indirect result of this. The decreased segregation would leave a higher carbon content within the grains, making precipitation of intragranular carbides more probable.

Additional support for the theory of equilibrium segregation is in the literature. Brown (ref. 46) proposed that boron additions beneficiated iron-base alloys by this mechanism. Strauss (ref. 47) emphasized that marked beneficiation of properties by trace-element additions usually occurs with elements with characteristics which would lead to segregation to grain boundaries.

Role of Carbon

The apparent harmful effect of $M_{23}C_6$ in the grain boundaries of the alloy and the possible helpful effect of the intragranular carbide promoted by boron make the role of carbon in nickel-base alloys of great interest.

One might conclude from the results that the relatively carbon-free alloy would be free of the grain boundary carbide agglomeration and, therefore, have properties equivalent to Heat V + B + Zr. This, however, is not the case. It has been shown in unpublished work at this laboratory that both rupture life and ductility increase as carbon is increased from less than 0.01 to 0.04 percent in the boron and zirconium-free alloy. Therefore, it seems that carbon can also have a beneficial role in the alloy. The reason for this effect is not at all clear at this time but it could be one of several mechanisms including improved degassing, solid-solution strengthening or prevention of other embrittling grain boundary reactions.

Generality of Results

The beneficial effects of boron and zirconium in nickel=base Ti + Al refractory alloys is common knowledge. Therefore, it follows that properties of such alloys in the absence of these elements will generally be inferior to their properties when the proper amounts are present. The particular alloy used to study the boron-zirconium mechanism is certainly not unusual in this respect. The results presented do in fact increase the confidence which can be placed in the alloy studied through clarification of the mechanism involved.

It is confidently expected that the basic mechanism established for the influence of trace amounts of boron and zirconium will be generally applicable. However, there will be variants in individual alloys and within a specific alloy depending on prior history, heat treatment and testing conditions. With this in mind, the limitations of the present results should be clearly recognized. Only one alloy with one heat treatment was studied. The test conditions were limited to $1600°F$ on material made in a small vacuum furnace and hot worked under idealized laboratory conditions.

In the type of alloy considered it is expected that boron and zirconium will generally be found to suppress the formation of non-coherent phases in grain boundaries and weakening of adjacent matrix material through depletion of γ'. Both the details of the mechanism and the effectiveness can be expected to vary depending on the major alloying elements in specific alloys and the variations of other elements in trace amounts. Because such factors as grain size, carbide composition and distribution and cold work are prior history sensitive, the effectiveness of the boron and zirconium can be expected to vary with the basic microstructure of the alloy. It should be recognized that the boron and zirconium must be present in an effective form. For instance, they must be added under conditions where their effectiveness is not nullified by reaction with oxygen or nitrogen.

The mechanism of creep can be expected to vary with test temperatures and stress. Conditions which favor creep within the grains (temperatures on the low side of the creep range and high stresses) apparently should reduce the effectiveness of boron and zirconium under the mechanism observed. Variations in the conditions of formation of γ' or in the amounts through variation in Ti and Al should also be involved. It is becoming evident through research efforts of others that the type of carbide formed can be temperature and time dependent. Again this should alter the effectiveness of the boron-zirconium reaction.

In reference 1 it was shown that there can be sharp optimums in the properties depending on the amounts of boron + zirconium. This aspect of the mechanism has not yet been established although it is expected that it will arise from some modification of the observed mechanism. This reference also showed that boron and zirconium up to limiting amounts were very effective in reducing cracking during hot working. This demonstrates that they are effective at temperatures much higher than 1600°F. It is not certain if the same mechanism observed at 1600°F is involved.

Boron, at least, is effective in raising creep-rupture properties of other types of alloys than the nickel-base Ti + Al bearing alloys. The results of this investigation suggest that it may operate in these cases through modification of carbide reactions. The further possibility also exists that boron, by itself or through modification of carbon-nitrogen reactions, introduces strain aging-type reactions.

CONCLUSIONS

Trace amounts of boron and zirconium increase creep-rupture properties of the complex Ti + Al hardened nickel-base alloy by retarding structural changes at the grain boundaries. In the absence of these elements, $M_{23}C_6$ and γ' agglomerate rapidly in the grain boundaries. Subsequently, the matrix material adjacent to the grain boundaries transverse to the applied stress becomes depleted of γ' precipitates. Micro-cracks then develop at the $M_{23}C_6$ - depleted matrix interfaces, grow and combine to initiate brittle and premature fracture.

Zirconium, boron and boron plus zirconium in the proper amounts retard these changes, with effectiveness increasing in the order listed, to allow longer life to higher deformations before fracture occurs. While micro-cracking was detected early in second-stage creep at relatively short time periods in the absence of boron and zirconium, proper amounts of boron and zirconium delayed micro-cracking until after third-stage creep started after long creep exposure.

Creep-rupture properties at 1600°F of the material correlated with the stability of the grain boundaries. The property effects were not found to result from a change in the size, amount and distribution of the general intragranular γ'.

Some possible causes of the stabilizing influence of boron and zirconium on the grain boundaries have been discussed. Of these, retardation of agglomeration by preferential segregation of boron and zirconium to grain boundaries fits the data best.

REFERENCES

1. Decker, R. F., Rowe, J. P., Freeman, J. W. : "Influence of Crucible Materials on High-Temperature Properties of Vacuum-Melted Nickel - Chromium - Cobalt Alloy." NACA TN 4049, June 1957.

2. Koffler, R. W., Pennington, W. J., Richmond, F. M. : "The Effect of Small Amounts of Boron and Zirconium on the High Temperature Properties of Vacuum-Melted Super Alloys." Report 48, Research and Development Department, Universal-Cyclops Steel Corporation, June 11, 1956.

3. Darmara, F. N. : "Quality Control Achieved by Vacuum Melting and Effects on High Temperature Properties." Paper presented at Regional High-Temperature Materials Conference of Cleveland Section of AIME, April 17, 1957.

4. Jones, W. E. : "Vacuum Induction Melting-Process Considerations." Metal Progress, Vol. 72, Oct. 1957, p. 133.

5. Nordheim, R., Grant, N. J. : "Aging Characteristics of Nickel-Chromium Alloys Hardened with Titanium and Aluminum." Journal of Metals, Vol. 6, 1954, p. 211.

6. Taylor, A. : "Constitution of Nickel-Rich Quaternary Alloys of the Ni - Cr - Ti - Al System." Journal of Metals, Vol. 8, 1956, p. 1356.

7. Betteridge, W., Franklin, A. W. : "Progress in Nickel-Chromium Base Alloys for Service at High Temperatures." Revue de Metallurgie, Vol. 53, 1956, p. 271. (French).

8. Frey, D. N., Freeman, J. W., White, A. E. : "Fundamental Aging Effects Influencing High-Temperature Properties of Solution Treated Inconel X." NACA TN 2385, 1951.

9. Brockway, L. O., Bigelow, W. C. : "The Investigation of the Minor Phases of Heat-Resistant Alloys by Electron Diffraction and Electron Microscopy." WADC TR 54-589, Wright-Patterson Air Force Base, Ohio, May 1955.

10. Betteridge, W., Smith, R. A. : "Effect of Heat Treatment and Structure Upon Creep Properties of Nimonic Alloys Between 750° and 950°C." Symposium on Metallic Materials for Service at Temperatures above 1600°F. ASTM, 1956, p. 29.

11. Baillie, Y. : "Some Results of an Electron Microscopic Study of Ni - Cr - Al - Ti Alloys Used in Aircraft Turbines." Revue Universelles des Mines, Vol. 12, 1956, p. 507. (French).

12. Beattie, H. J., VerSnyder, F. L. : "The Influence of Molybdenum on the Phase Relationships of a High Temperature Alloy." Trans. ASM, Vol. 49, 1957, p. 883.

13. Wilde, R. F., Grant, N. J. : "Aging in Complex Commercial Ni - Cr Alloys Hardened with Titanium and Aluminum." Journal of Metals, Vol. 9, 1957, p. 865.

14. Betteridge, W., Franklin, A. W. : "The Effect of Heat-Treatment and Structure on The Creep and Stress-Rupture Properties of Nimonic 80A." Journal Inst. Metals, Vol. 85, 1957, p. 473.

15. Bigelow, W. C., Amy, J. A., Brockway, L. O. : "Electron Microscopic Identification of the γ' Phase of Nickel-Base Alloys." Proc. ASTM, Vol. 56, 1956, p. 945.

16. Fisher, R. M. : "Electron Microstructure of Steels by Extraction Replica Technique." Symposium on Techniques for Electron Metallography, ASTM, 1953, p. 49.

17. Plateau, J., Henry, G., Crussard, C. : "Some New Applications of Microfractography." Revue de Metallurgie, Vol. 54, 1957, p. 200. (French).

18. Bradley, D. E. : "Evaporated Carbon Films for Use in Electron Microscopy." British Journal of Applied Physics, Vol. 5, 1954, p. 65.

19. Fullam, E. F. : "Replica Washing Methods." Symposium on Techniques for Electron Metallography, ASTM, 1953, p. 101.

20. Cottrell, A. H. : "Creep and Aging Effects in Solid Solutions." Creep and Fracture of Metals at High Temperatures. Her Majesty's Stationery Office, London, 1956, p. 141.

21. Wache, X. : "Discontinuous Elongation of Austenitic - 80 Nickel, 20 Chromium Alloy and Elinvar Subjected to an Ordinary Tensile Test at High Temperature." Comptes Rendus, Vol. 240, 1955, p. 1892. (French).

22. Buckle, Ch., Poulignier, J. : "A Metallographic Study of Cold Working on Heat Resisting 80-20 Nickel-Chromium Alloys." Revue de Metallurgie, Vol. 53, March 1956, p. 179. (French).

23. Simpkinson, T. V. : "Metallography of Titanium-Stabilized 18-8 Stainless Steels." Trans. ASM, Vol. 39, 1947, p. 721.

24. Bungardt, K., Lennartz, G. : Arch. Eisen, Vol. 27, 1956, p. 127. (German).

25. Baillie, Y., Poulignier, J. : "Submicroscopic Precipitation in Heat-Resistant Nickel-Chromium Alloys." Revue de Metallurgie, Vol. 51, 1954, p. 179. (French).

26. Mathieu, M. : "Contribution to the Knowledge of Modified Heat-Resistant 80 Ni - 20 Cr Alloys." La Recherche Aeronautique, Vol. 51, May-June 1956, p. 43. (French).

27. Chang, H. C., Grant, N. J. : "Mechanism of Intercrystalline Fracture," Journal of Metals, Vol. 8, 1956, p. 544.

28. Wever, F., Schrader, H. : "Electron Microscopy of Changes in Structure of Cr - Ni - Mo Steel Under Long-Time Tension Stress at 500°C." Arch. Eisen., Vol. 26, 1955, p. 475. (German).

29. Roberts, C. S. : "Interaction of Precipitation and Creep in Mg - Al Alloys." Journal of Metals, Vol. 8, 1956, p. 146.

30. Sully, A. H. : Discussion in Creep and Fracture of Metals at High Temperatures. Her Majesty's Stationery Office, London, 1956, p. 308.

31. Resnick, R., Seigle, L. : "Nucleation of Voids in Metals During Diffusion and Creep." Journal of Metals, Vol. 9, 1957, p. 87.

32. Machlin, E. S. : "Creep-Rupture by Vacancy Condensation." Journal of Metals, Vol. 8, 1956, p. 106.

33. Greenwood, J. N., Miller, D. R., Suiter, J. W. : "Intergranular Cavitation in Stressed Metals." Acta Metallurgica, Vol. 2, 1954, p. 250.

34. Crussard, C., Friedel, J. : "Theory of Accelerated Creep and Rupture." Creep and Fracture of Metals at High Temperatures. Her Majesty's Stationery Office, London, 1956, p. 243.

35. Guy, A. G. : "Russian Theory for Creep Fracture." Metal Progress, Vol. 69, March 1956, p. 158.

36. McLean, D. : "A Note on the Metallography of Cracking During Creep." Journal Inst. Metals, Vol. 85, 1957, p. 468.

37. Nield, B. J., Quarrell, A. G. : "Intercrystalline Cracking in Creep of Some Aluminum Alloys." Journal Inst. Metals, Vol. 85, 1957, p. 480.

38. Nield, B. J. : Discussion in Creep and Fracture of Metals at High Temperatures. Her Majesty's Stationery Office, London, 1956, p. 308.

39. Kishkin, S. T. : "Mechanism of Weakening and Fracture of Crystalline Bodies as a Function of Time at High Temperature." Doklady Akademii Nauk SSSR, Vol. 95, 1954, p. 789. (Russian).

40. McAdam, D. J., Giel, G. W., Woodard, D. H. "Influence of Strain Rate and Temperature on the Mechanical Properties of Monel Metal and Copper." Proc. ASTM, Vol. 46, 1946, p. 902.

41. Kirkby, H. W. : "Discussion in Creep and Fracture of Metals at High Temperatures. Her Majesty's Stationery Office, London, 1956, p. 331.

42. Dekhtiar, I. I., Osipov, K. A. : "Fracture of Metals at High Temperatures." Doklady Akademii Nauk SSSR, Vol. 104, 1955, p. 229. (Russian).

43. Cahn, R. W. : "Grain Boundaries, Substructures and Impurities." Impurities and Imperfections. ASM, 1955, p. 41.

44. Thomas, W. R., Chalmers, B. : "The Segregation of Impurities to Grain Boundaries." Acta Metallurgica, Vol. 3, Jan. 1955, p. 17.

45. Speiser, R., Spretnak J. W., Taylor, W. J. : "Effective Diameter of Solute Atoms in Interstitial Solid Solution." Trans. ASM, Vol. 46, 1954, p. 1168.

46. Brown, J. T., Bulina, J. : "W-545 - A New High Temperature Turbine Disc Alloy." Paper presented at Regional High-Temperature Materials Conference of Cleveland Section of AIME, April 16, 1957.

47. Strauss, J. : "Micrometallurgy - The Metallurgy of Minute Additions." Proc. ASTM, Vol. 53, 1953, p. 577.

TABLE I

Chemical Analyses of Experimental Heats

(weight percent as rolled)

Heat	B	Zr	Cr	Co	Mo	Ti	Al	Si	Mn	C	S	P	Mg	Fe	Cu
V	.0002	<.01	19.7	15.0	3.90	3.08	3.35	.17	.13	.08	.007	.006	<.01	<.30	<.10
V + Zr	.0004	.19	18.8	15.1	4.15	3.14	3.14	.10	<.10	.08	.008	.003	--	<.30	--
V + B	.0089 .0090[1] .0079[2]	<.01	20.9	14.8	4.20	3.15	3.25	.20	<.10	.10	--	.004	<.01	<.30	<.10
V + B + Zr	.0088	.01	20.8	14.8	4.20	3.20	3.30	.19	.11	.09	--	.007	<.01	<.30	<.10

1. Analysis on cross section of 0.250-inch diameter rupture specimen after 428 hours at 1600°F.

2. Analysis on 0.010-inch surface layer of sample described in 1.

TABLE II

Creep-Rupture Data at 1600°F

(Initial Condition - 2 hours at 2150°F, air cooled + 4 hours preheat at 1600°F before loading)

Heat	Stress (psi)	Minimum Second Stage Creep Rate (%/hr)	Rupture Time (hr)	Elongation (%)	Reduction of Area (%)	Interruption Time (hr)	Total Deformation (%)
V	25,000	0.0160	45	2	1	--	--
	25,000	0.0060	52	2	1	--	--
	20,000	0.0070	158	3	2	--	--
	20,000	0.0040	--	--	--	165	1.23
	20,000	0.0058	--	--	--	117	1.00
	20,000	0.0046	--	--	--	85	0.76
	20,000	0.0052	--	--	--	85	0.76
	20,000	0.0084	--	--	--	47	0.55
	20,000	0.0058	--	--	--	23	0.29
V + Zr	25,000	0.0036	147	5	5	--	--
	25,000	0.0095	134	6	8	--	--
	22,500	0.0032	208	5	4	--	--
	22,500	0.0036	--	--	--	172	1.25
	20,000	0.0027	--	--	--	165	0.63
V + B	28,000	0.0025	296	10	14	--	--
	28,000	0.0040	--	--	--	214	3.45
	28,000	--	--	--	--	188	1.21
	28,000	0.0046	--	--	--	68	0.56
	25,000	0.0018	429	10	11	--	--
	25,000	--	394	7	8	--	--
	20,000	negative	--	--	--	165	0.15
V + B + Zr	30,000	0.0021	266	8	9	--	--
	30,000	--	--	--	--	214	1.18
	25,000	0.0004	666	17	16	--	--
	25,000	0.0003	627	12	13	--	--
	20,000	negative	--	--	--	165	0.04

TABLE III

Properties of Specimens Stress Aged at 1600°F

Condition	Heat V Nodules[1]	Heat V γ' density[2]	Heat V Depleted Grain Boundaries	Heat V Micro-cracks	Heat V + Zr Nodules	Heat V + Zr γ' density	Heat V + Zr Depleted Grain Boundaries	Heat V + Zr Micro-cracks	Heat V + B Nodules	Heat V + B γ' density	Heat V + B Depleted Grain Boundaries	Heat V + B Micro-cracks	Heat V + B + Zr Nodules	Heat V + B + Zr γ' density	Heat V + B + Zr Depleted Grain Boundaries	Heat V + B + Zr Micro-cracks
Equal Strain Rate Study																
0.3% creep deformation	239	--	49	5	--	--	--	--	--	--	--	--	--	--	--	--
0.6% creep deformation	301	--	76	17	--	--	--	--	5	--	2	2	--	--	--	--
0.8% creep deformation	332 288	--	184 173	34 31	-- --	-- --	-- --	-- --	-- --	-- --	-- --	-- --	-- --	-- --	-- --	-- --
1.0% creep deformation	334	--	151	--	--	--	--	--	--	--	--	--	--	--	--	--
1.2% creep deformation	418	134	264	314	175	137	127	78	63	157	60	30	20	117	23	2
3.5% creep deformation	--	--	--	--	--	--	--	--	79	--	165	77	--	--	--	--
ruptured	532	--	764	958	228	--	568	532	176	--	676	243	86	--	538	198
Equal Stress Study																
165 hours at 20,000 psi	418	134	264	314	129	151	72	9	25	158	16	none detected	0	125	none detected	none detected
ruptured at 25,000 psi	225 218	256 --	192 211	374 378	254 --	109 --	916 --	145 --	145 --	67 --	442 --	166 --	86 90	51 --	661 530	402 330

1. Mixed carbide and γ' nodule greater than 5 microns diameter, number in 0.008 square inches.
2. γ' particles per square inch at 12,000D.
3. Grain boundaries where depletion was detected at 1000D, number in 0.008 square inches.
1. Micro-cracks detected at 1000D, number in 0.008 square inches.

TABLE IV

Properties of Specimens Aged at 1600°F Without Stress

Aging Time (hr)	Heat V DPH	Heat V Nodules[1]	Heat V γ' density[2]	Heat V + Zr DPH	Heat V + Zr Nodules	Heat V + Zr γ' density	Heat V + B DPH	Heat V + B Nodules	Heat V + B γ' density	Heat V + B + Zr DPH	Heat V + B + Zr Nodules	Heat V + B + Zr γ' density
0.5	359	--	--	354	--	--	357	--	--	373	--	--
1	364	--	--	362	--	--	362	--	--	380	--	--
4	359	--	--	353	--	--	357	--	--	366	--	--
10	355	45	588	348	32	544	348	16	768	362	0	584
100	345	180	134	346	57	147	346	33	168	355	19	137
188	338	--	107	342	--	116	340	--	101	353	--	103
500	335	300	65	344	139	67	339	149	68	344	25	64

1   Nodules greater than 5 microns diameter, number in 0.008 square inches.

2   γ' particles per square inch at 12,000D.
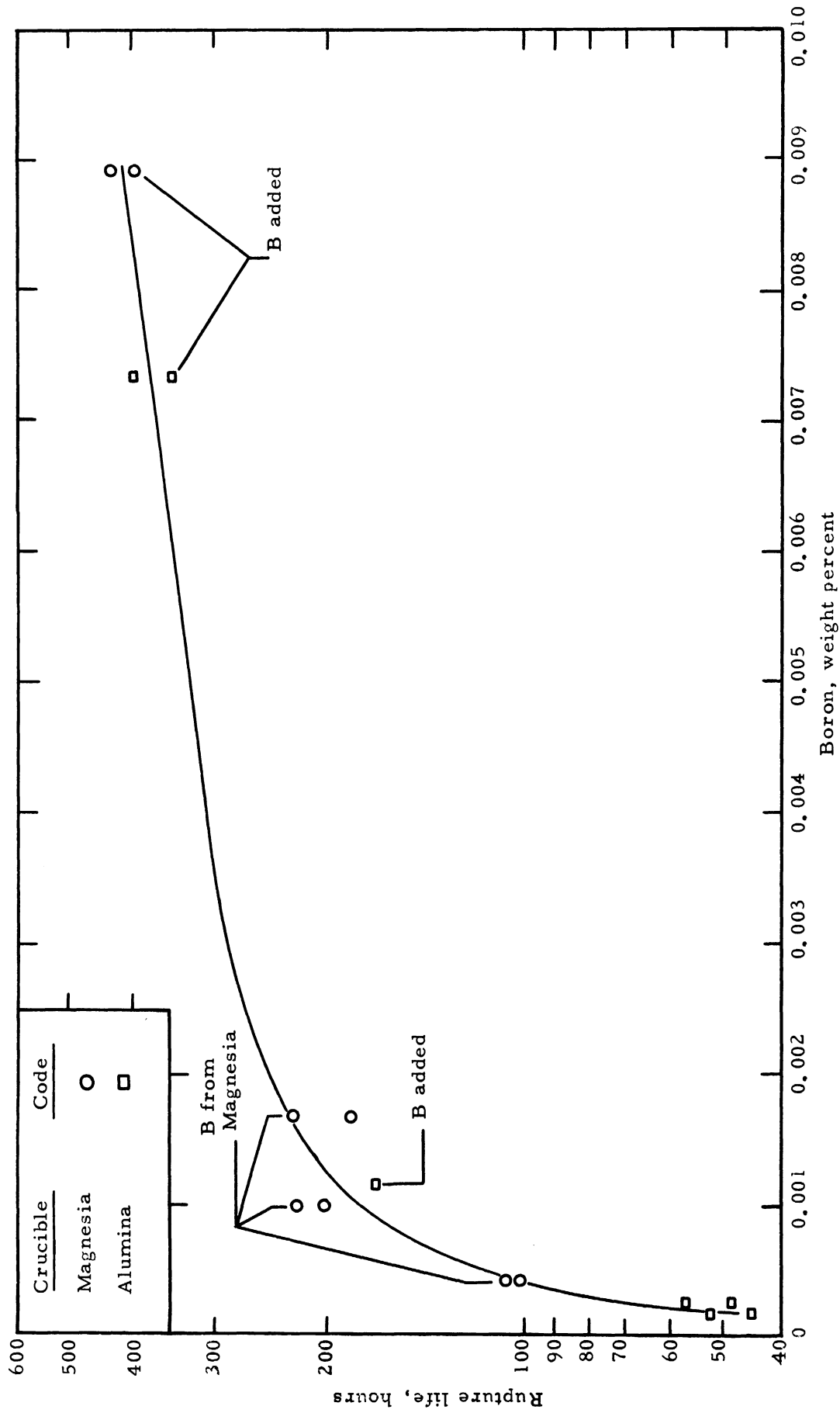
Figure 1. – Effect of boron content on rupture life at 1600°F and 25,000 psi of experimental heats of 55 Ni – 20 Cr – 15 Co – 4 Mo – 3 Ti – 3 Al alloy (with less than 0.01% Zr). Heat treatment prior to testing was 2 hours at 2150°F, air cooled plus 4 hours preheat at 1600°F. Decker, Rowe and Freeman (ref. 1).
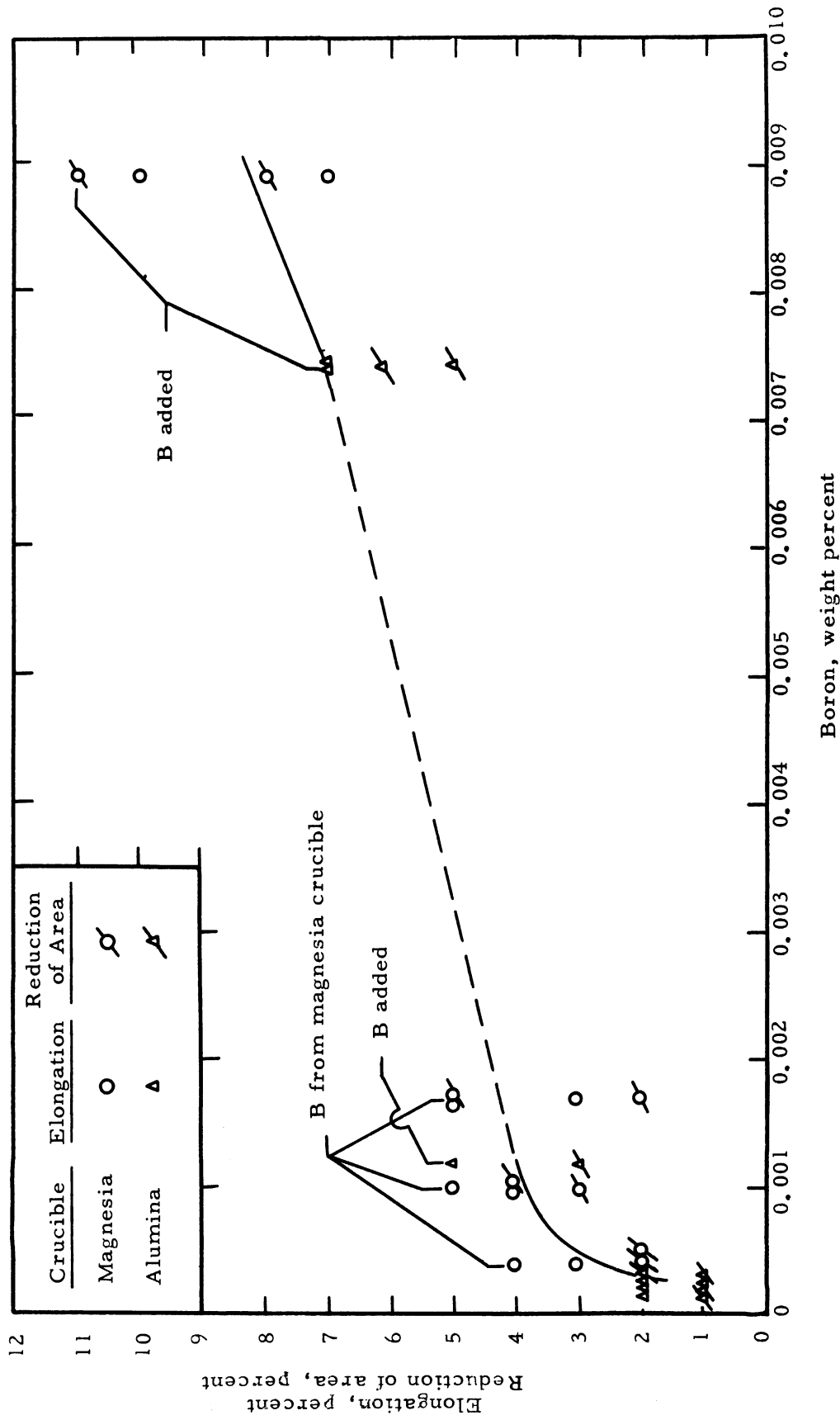
Figure 2. - Effect of boron content on ductility at 1600°F and 25,000 psi of experimental heats of 55 Ni - 20 Cr - 15 Co - 4 Mo - 3 Ti - 3 Al alloy (with less than 0.01% Zr). Heat treatment prior to testing was 2 hours at 2150°F, air cooled plus 4 hours preheat at 1600°F. Decker, Rowe and Freeman (ref. 1).
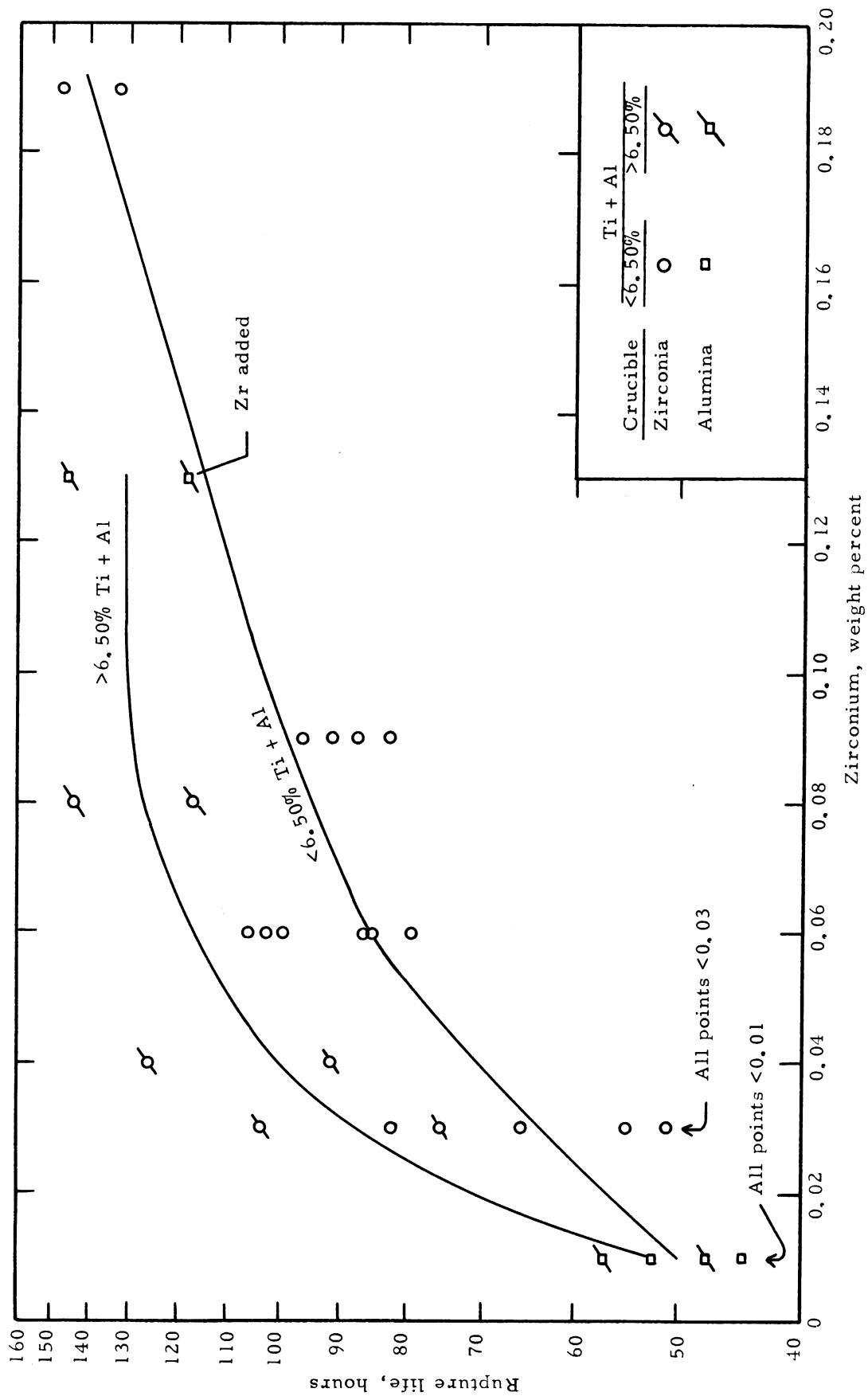
Figure 3. — Effect of zirconium content on rupture life at 1600°F and 25,000 psi of experimental 55 Ni - 20 Cr - 15 Co - 4 Mo - 3 Ti - 3 Al alloy (with less than 0.0005% B). Heat treatment prior to testing was 2 hours at 2150°F, air cooled plus 4 hours preheat at 1600°F. Decker, Rowe and Freeman (ref. 1).
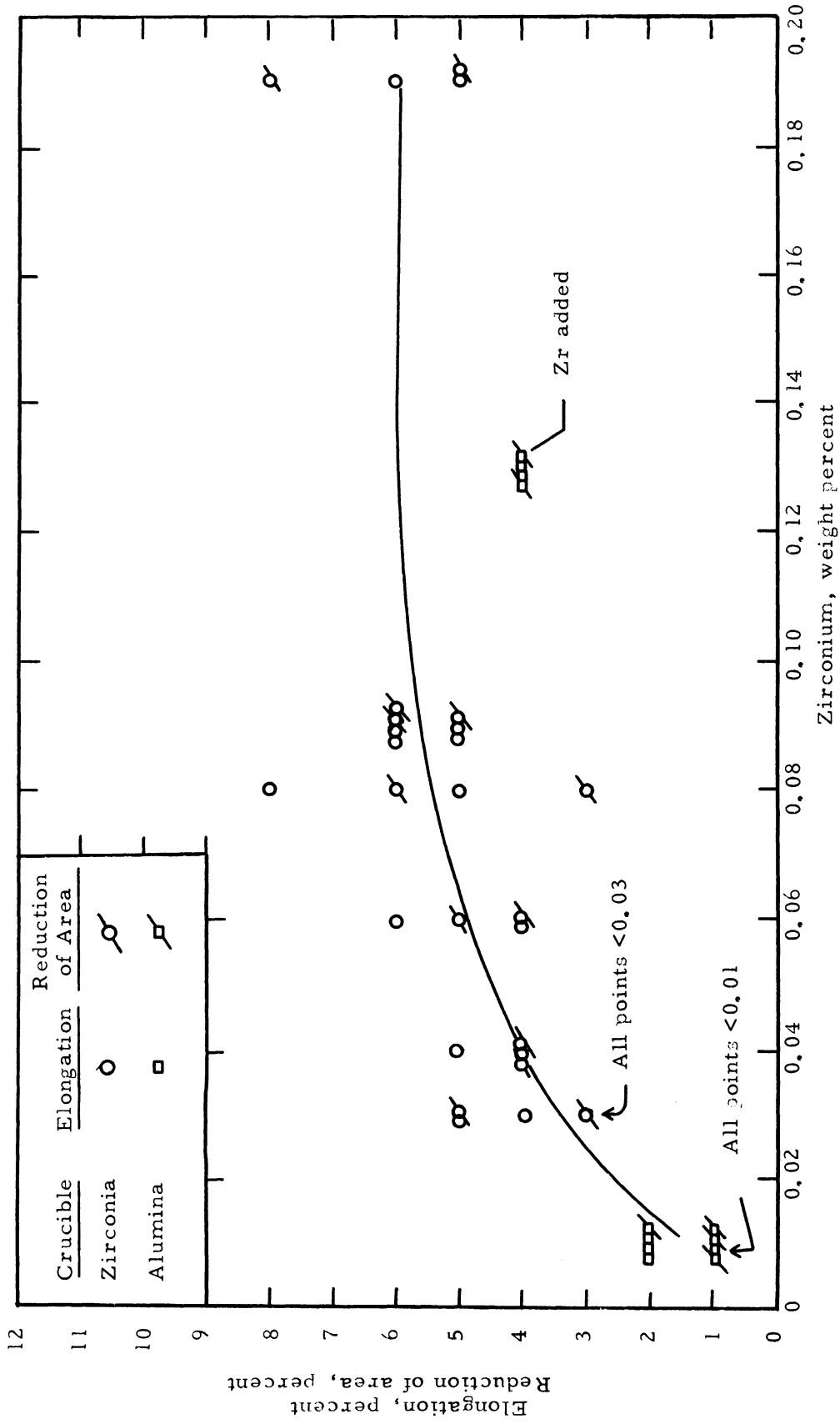
Figure 4. - Effect of zirconium content on ductility at 1600°F and 25,000 psi of experimental heats of 55 Ni - 20 Cr - 15 Co - 4 Mo - 3 Ti - 3 Al alloy (with less than 0.0005% B and between 0.04 to 0.09% C). Heat treatment prior to testing was 2 hours at 2150°F, air cooled plus 4 hours preheat at 1600°F. Decker, Rowe and Freeman (ref. 1).

Code	Heat	B	Zr
□	V	0.0002	<0.01
○	V + Zr	0.0004	0.19
◁	V + B	0.0089	<0.01
▷	V + B + Zr	0.0088	0.01

Minimum second stage creep rate, percent per hour

Stress, psi
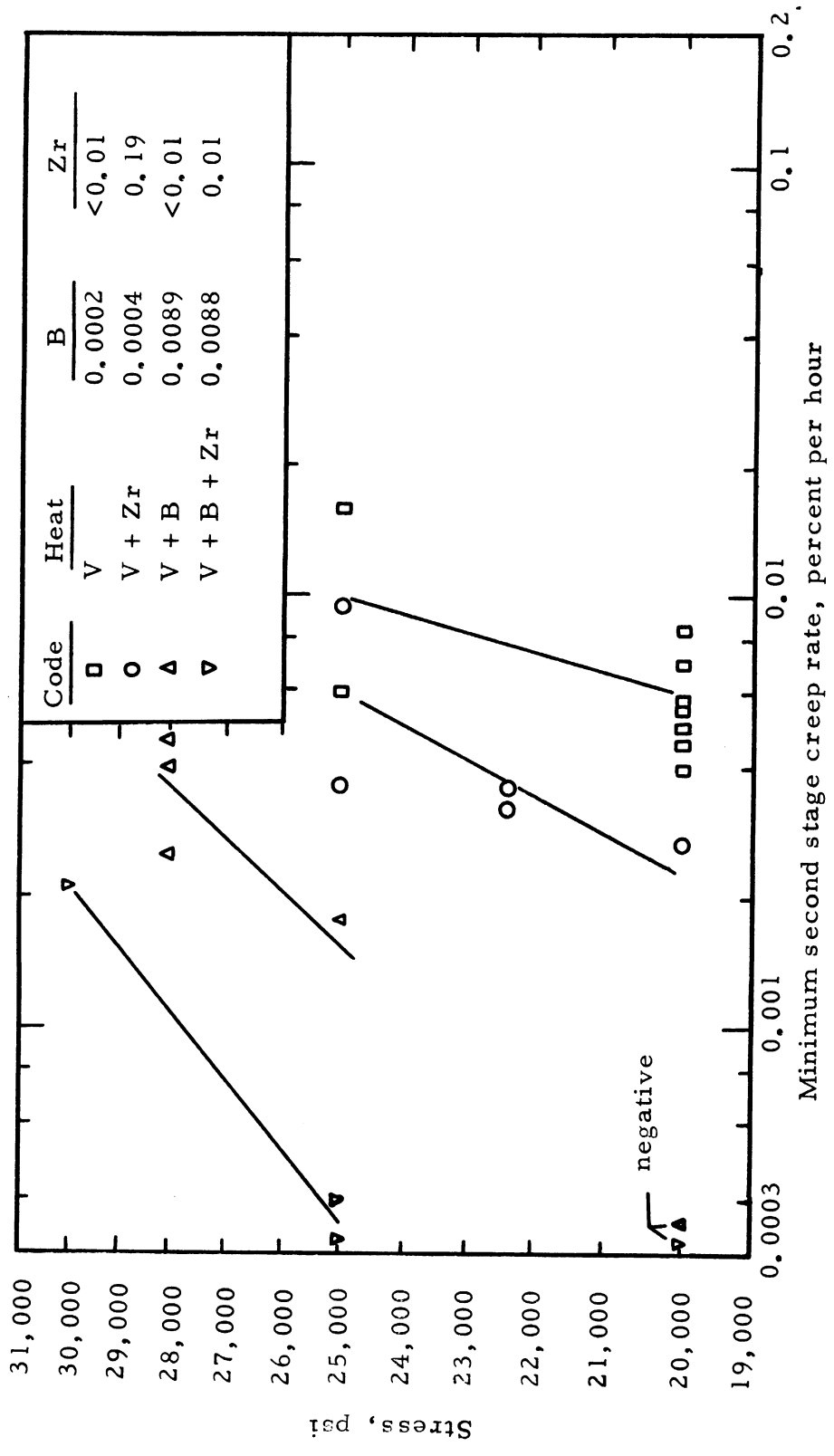
Figure 5. - Influence of stress on minimum second stage creep rate at 1600°F for the experimental heats.
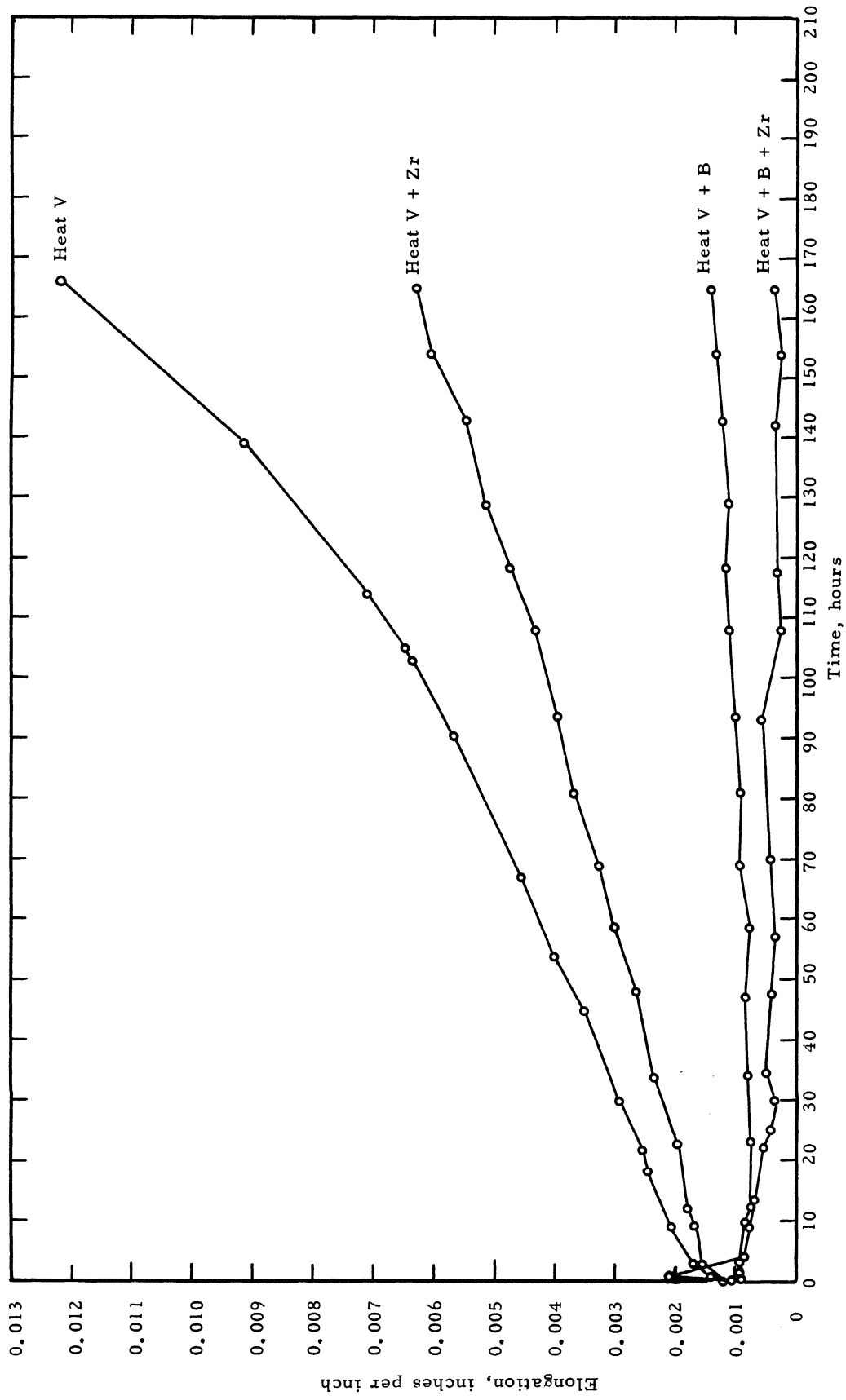
Figure 6. - Comparative creep curves at 1600°F and 20,000 psi for experimental heats.
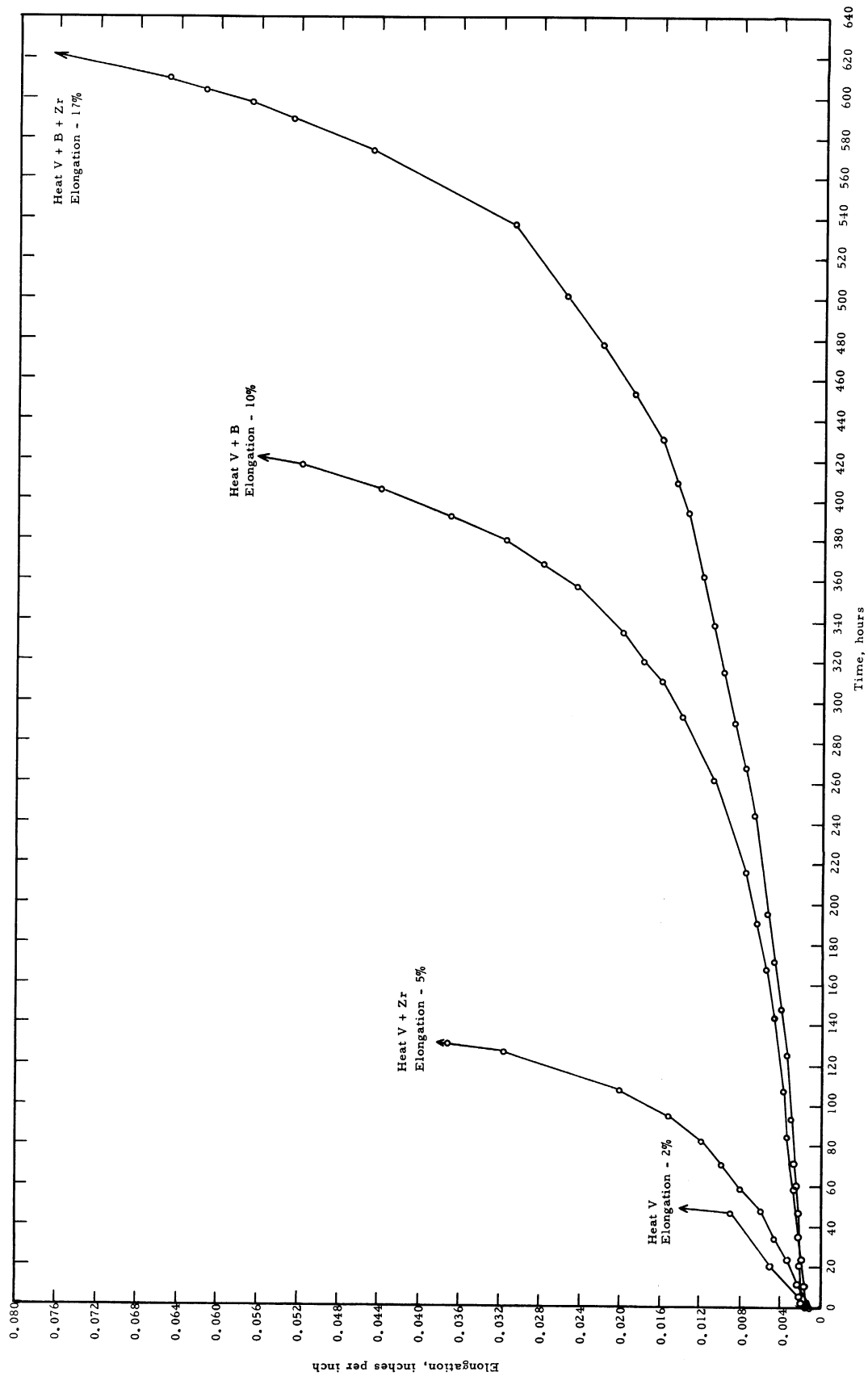
Figure 7. - Comparative creep curves at 1600°F and 25,000 psi for experimental heats.
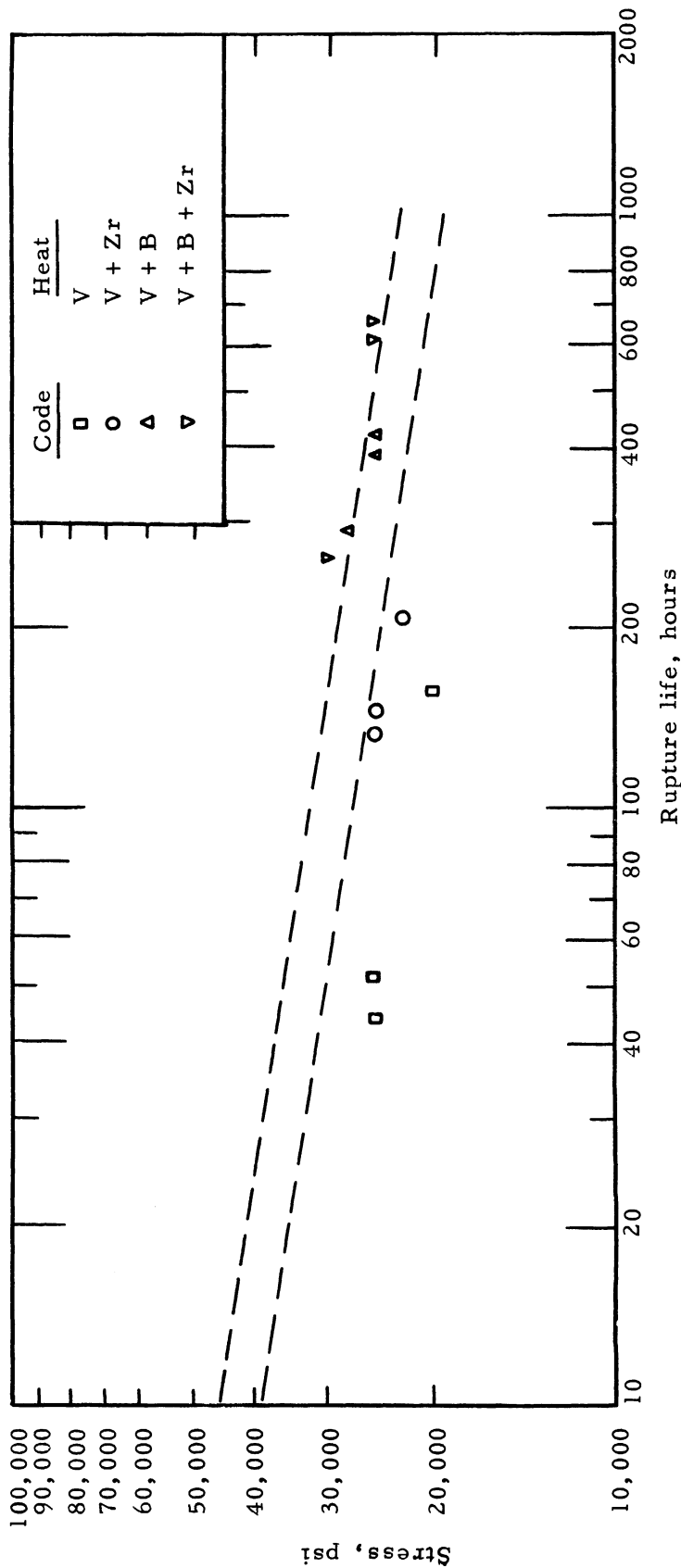
Figure 8. - Effect of stress on rupture life of experimental alloys at 1600°F. Treatment prior to testing was 2 hours at 2150°F, air cooled plus 4 hours preheat at 1600°F. Data plotted on dashed rupture band for two heats of commercial 55 Ni - 20 Cr - 15 Co - 4 Mo - 3 Ti - 3 Al alloy (Udimet 500) as reported by Utica Drop Forge and Tool Division of Kelsey-Hayes Company. Heat treatment for commercial alloy was 2 hours at 2150°F, air cooled; plus 4 hours at 1975°F, air cooled; plus 24 hours at 1550°F, air cooled; plus 16 hours at 1400°F, air cooled.
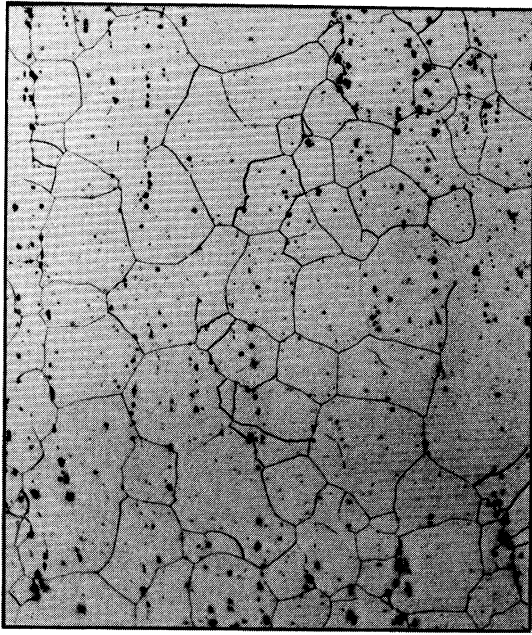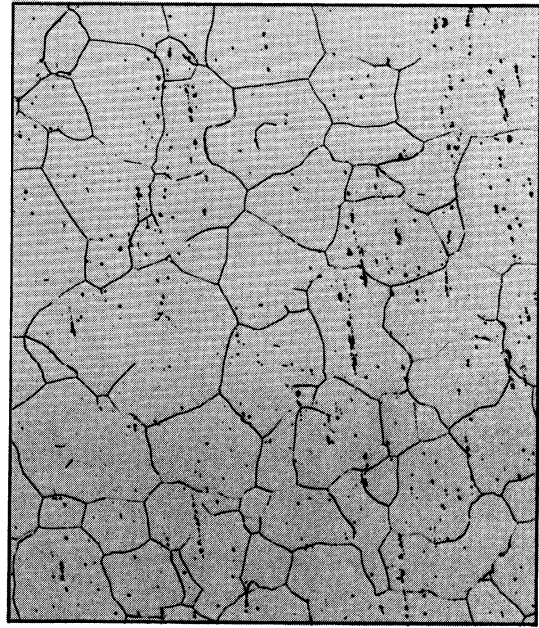
a. Heat V.   DPH-354   b. Heat V + Zr.   DPH-353
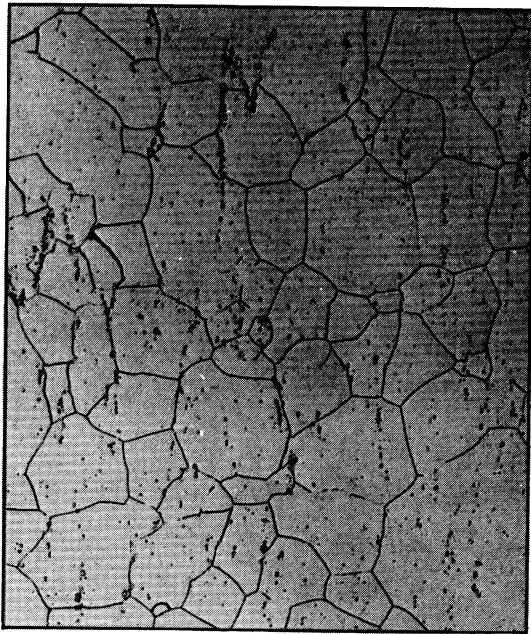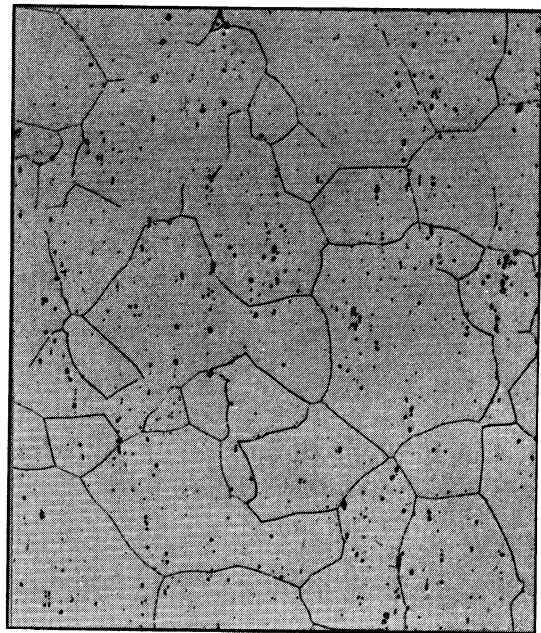
c. Heat V + B.   DPH-345   d. Heat V + B + Zr.   DPH-348

Figure 9. -   Initial condition of experimental heats as treated 2 hours
at 2150°F, air cooled. X100D.
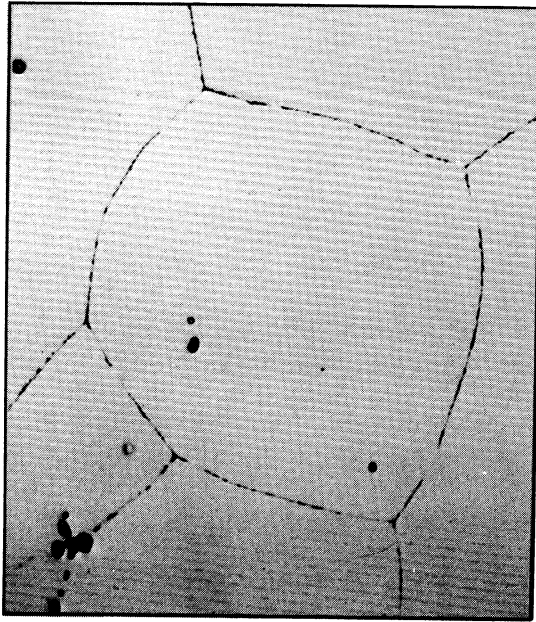
a. Heat V.
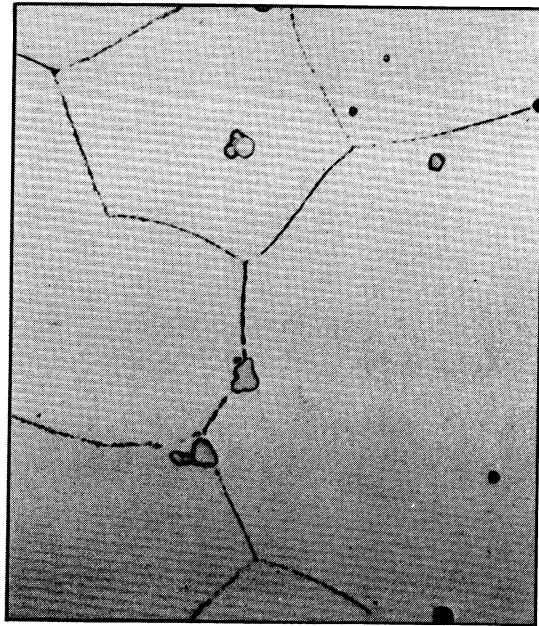
b. Heat V + Zr.
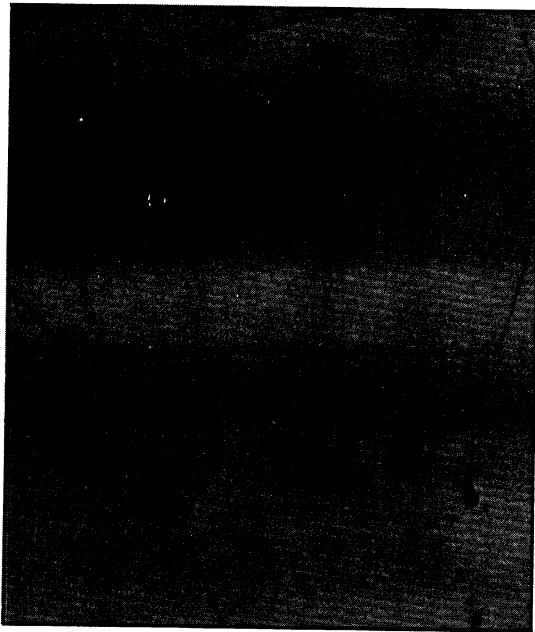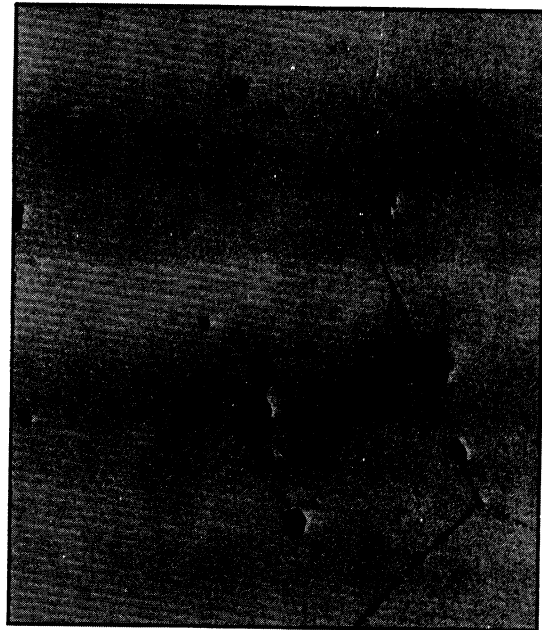
c. Heat V + B.

d. Heat V + B + Zr.

Figure 10. -   Initial condition of experimental heats as treated 2 hours
                 at 2150°F, air cooled. X1000D.

a. Heat V.

b. Heat V + Zr.
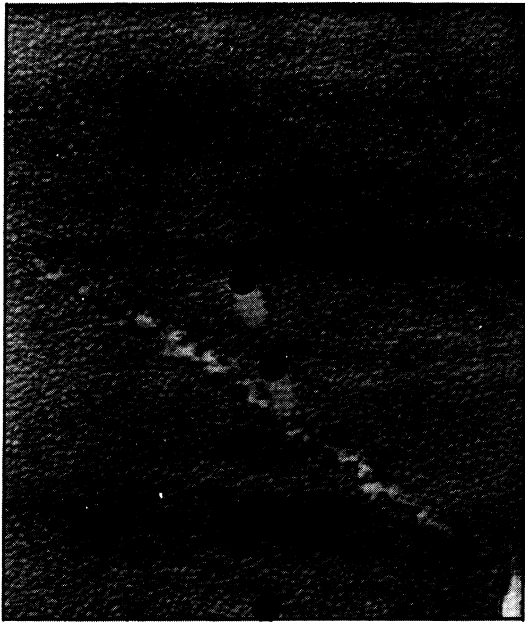
c. Heat V + B.

d. Heat V + B + Zr.

Figure 11. - Initial condition of experimental heats as treated 2 hours at 2150°F, air cooled. Electron micrographs X12,000D.
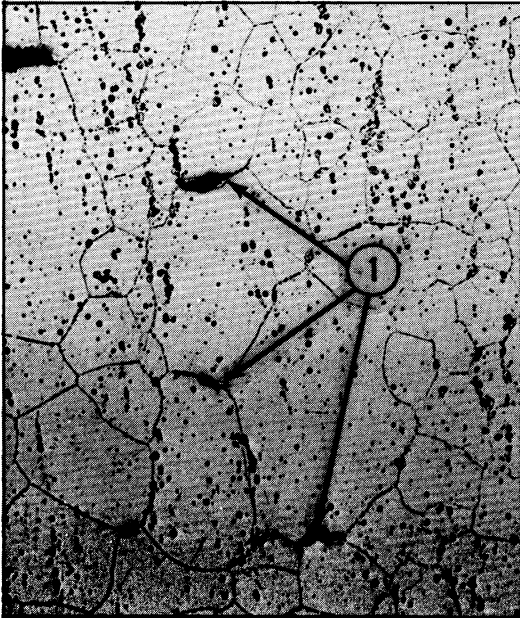
a. Heat V.
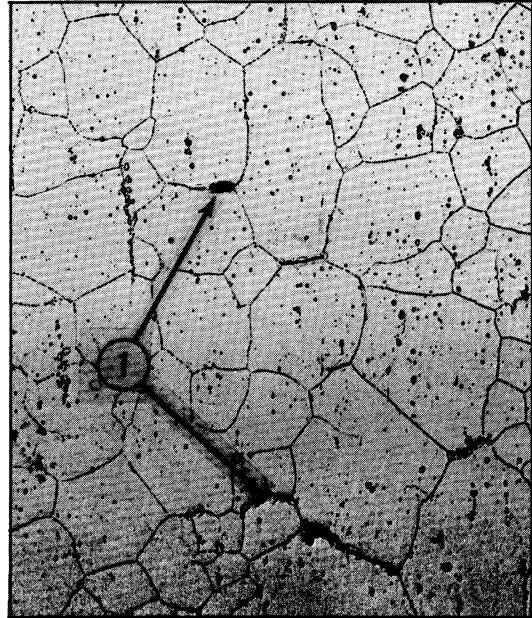
b. Heat V + Zr.
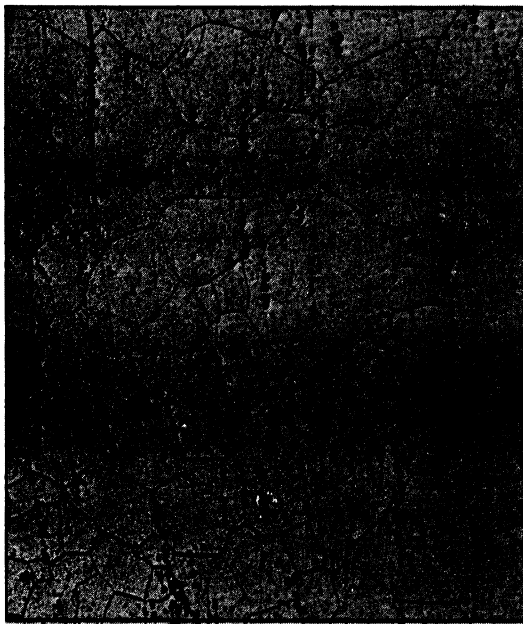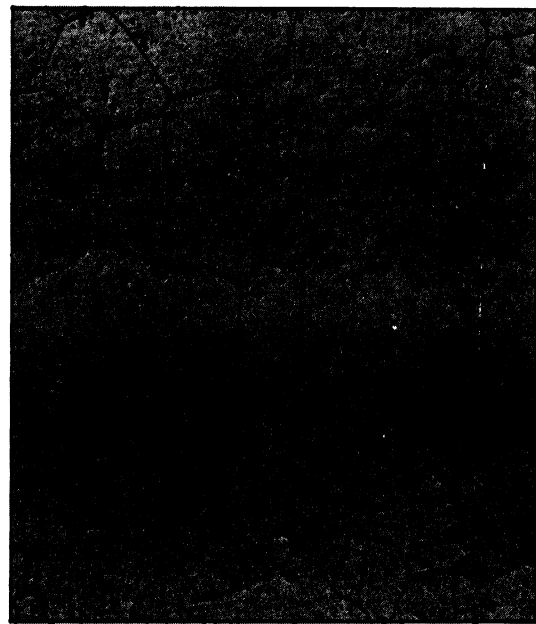
c. Heat V + B.

d. Heat V + B + Zr.

Figure 12. -   Microstructures of experimental heats after 1.2 percent
deformation by creep at 1600°F in 165-214 hours. Electro-
polished. X100D. ① - micro-crack.
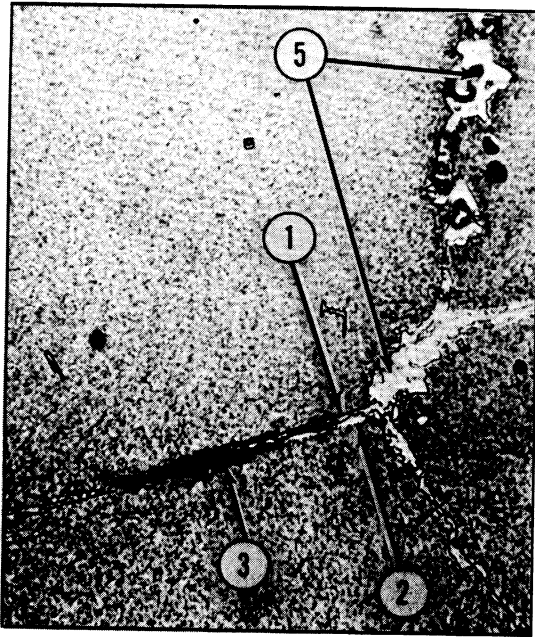
a. Heat V.   Heat V + Zr.
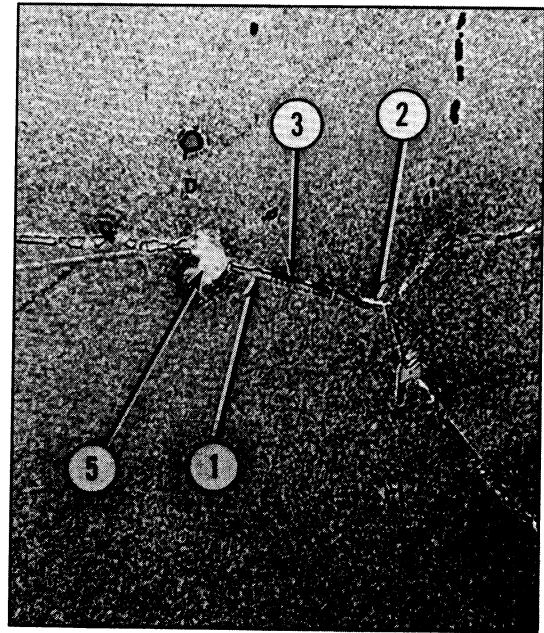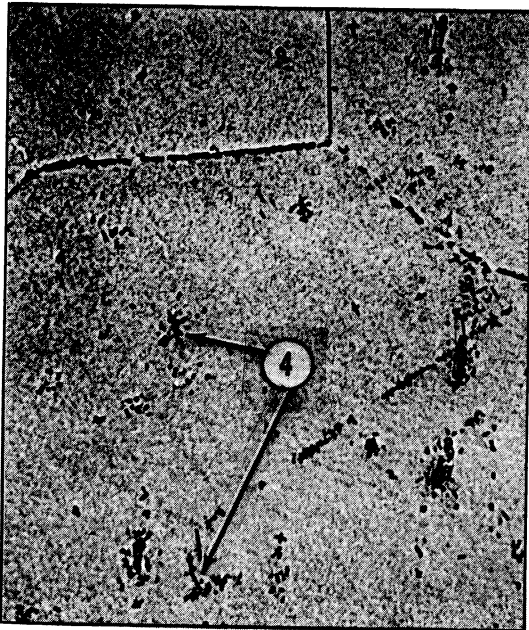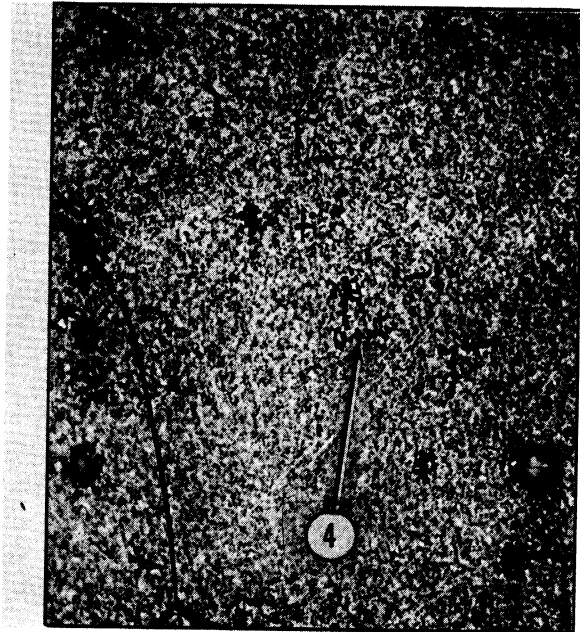
c. Heat V + B.   d. Heat V + B + Zr.

Figure 13.   -   Microstructures of experimental heats after 1.2 percent
deformation by creep at 1600°F in 165-214 hours. X1000D.
①- intergranular $M_{23}C_6$; ②- depleted grain boundary; ③-
micro-crack; ④- intragranular carbide; ⑤- nodule.
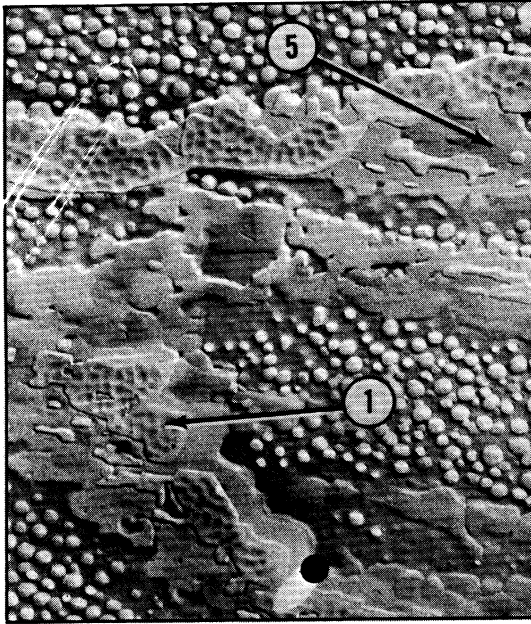
a. Heat V, typical grain
    boundaries.
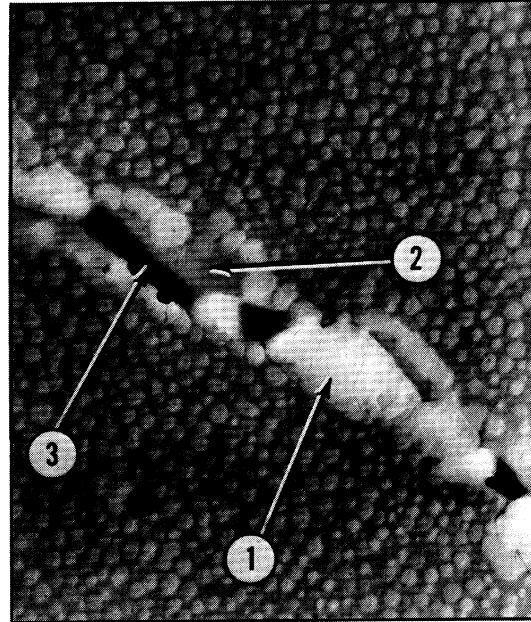
b. Heat V + Zr, depleted and
    cracked grain boundary with
    typical $M_{23}C_6$ precipitate.
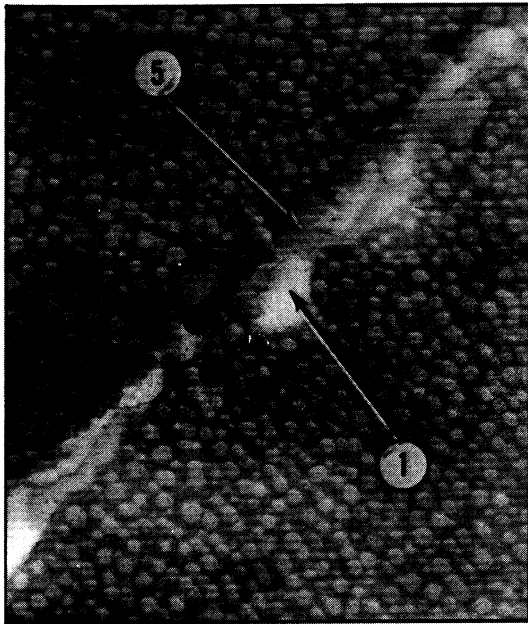
c. Heat V + B, typical grain
    boundary.
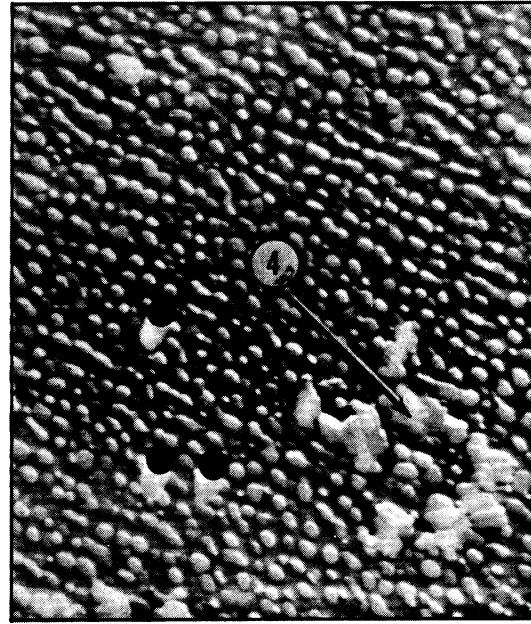
d. Heat V + B, intragranular carbides
    and alignment of γ'.

Figure 14. - Microstructures of experimental heats after 1.2 percent
deformation by creep at 1600°F in 165-214 hours. Electron
micrographs X12,000D. (1) - intergranular $M_{23}C_6$; (2) -
depleted grain boundary; (3) - micro-crack; (4) - intragranular
carbide; (5) - γ'; (6) - Ti(C,N).
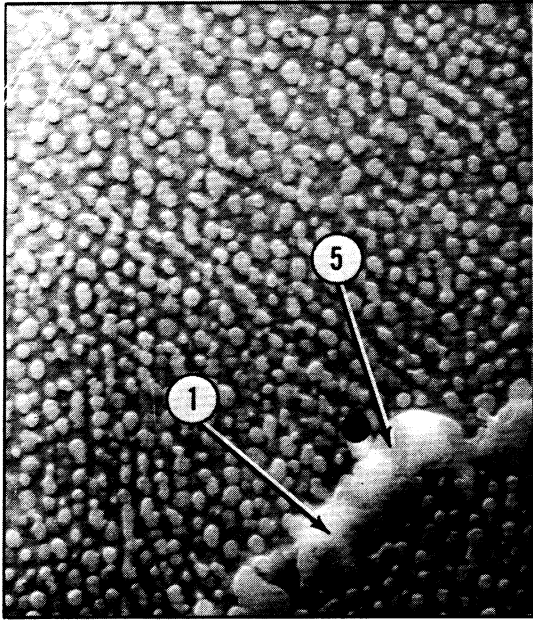
e. Heat V + B + Zr, typical
   grain boundary and alignment
   of γ'.
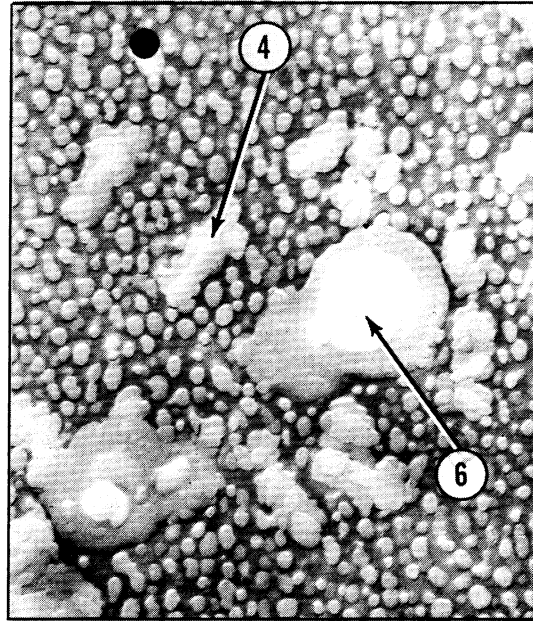
f. Heat V + B + Zr, intragranular
   carbides surrounding Ti(C, N).

Figure 14. - concluded.

X8000D

a. Extraction replica of carbide
from intergranular fracture
surface of Heat V after 1.2
percent creep deformation in
165 hours at 1600°F. All
selected area electron diffra-
tion spots indexed as $M_{23}C_6$.
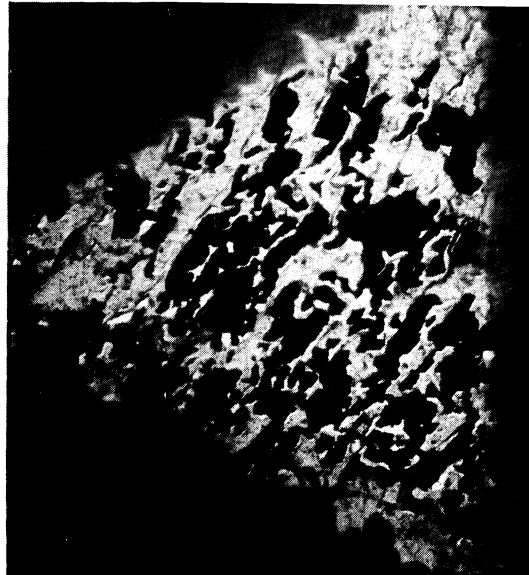
X8000D

b. Extraction replica of carbide from
intergranular fracture surface of
Heat V + B after 1.2 percent creep
deformation in 188 hours at 1600°F.
All selected area electron diffraction
spots indexed as $M_{23}C_6$.
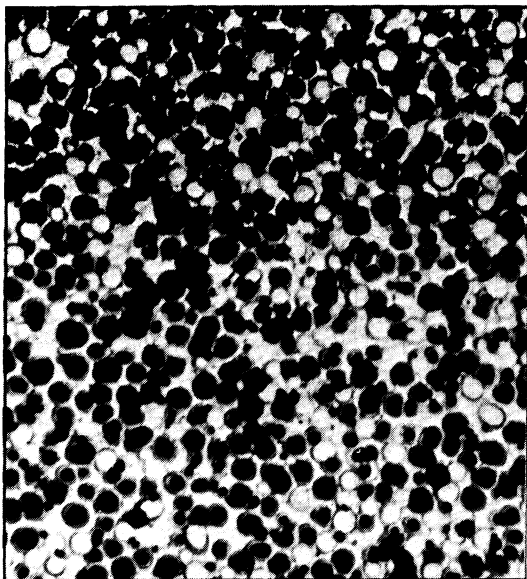
X36,000D

c. Extraction replica of intra-
granular γ' from Heat V + Zr
after aging 10 hours at 1600°F.
All selected area electron diffra-
tion spots indexed as γ'.
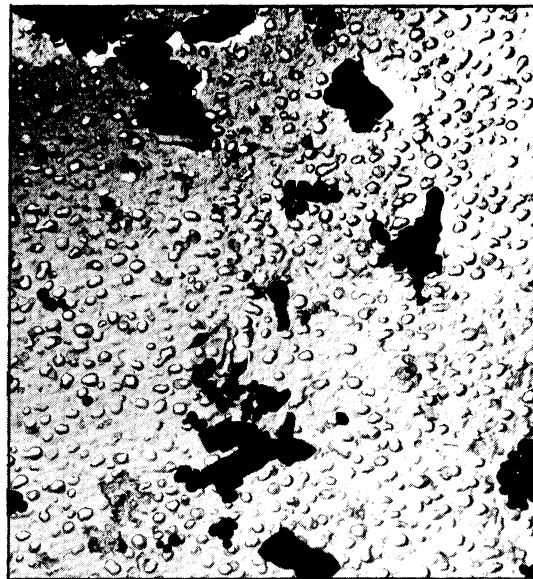
X8000D

d. Extraction replica of intragranular
carbide from Heat V + B after 1.2
percent creep deformation in 188
hours at 1600°F. Most selected area
electron diffraction spots indexed as
M_6C; a few as $M_{23}C_6$.

Figure 15. - Micrographs of phases extracted from the experiméntal heats.
Extracted particles appear black.

X2000D
Light micrograph

X12,000D
Electron micrograph

| Code		
Interrupted	Ruptured	Heat
□	■	V
O	●	V + Zr
△	▲	V + B
▽	▼	V + B + Zr
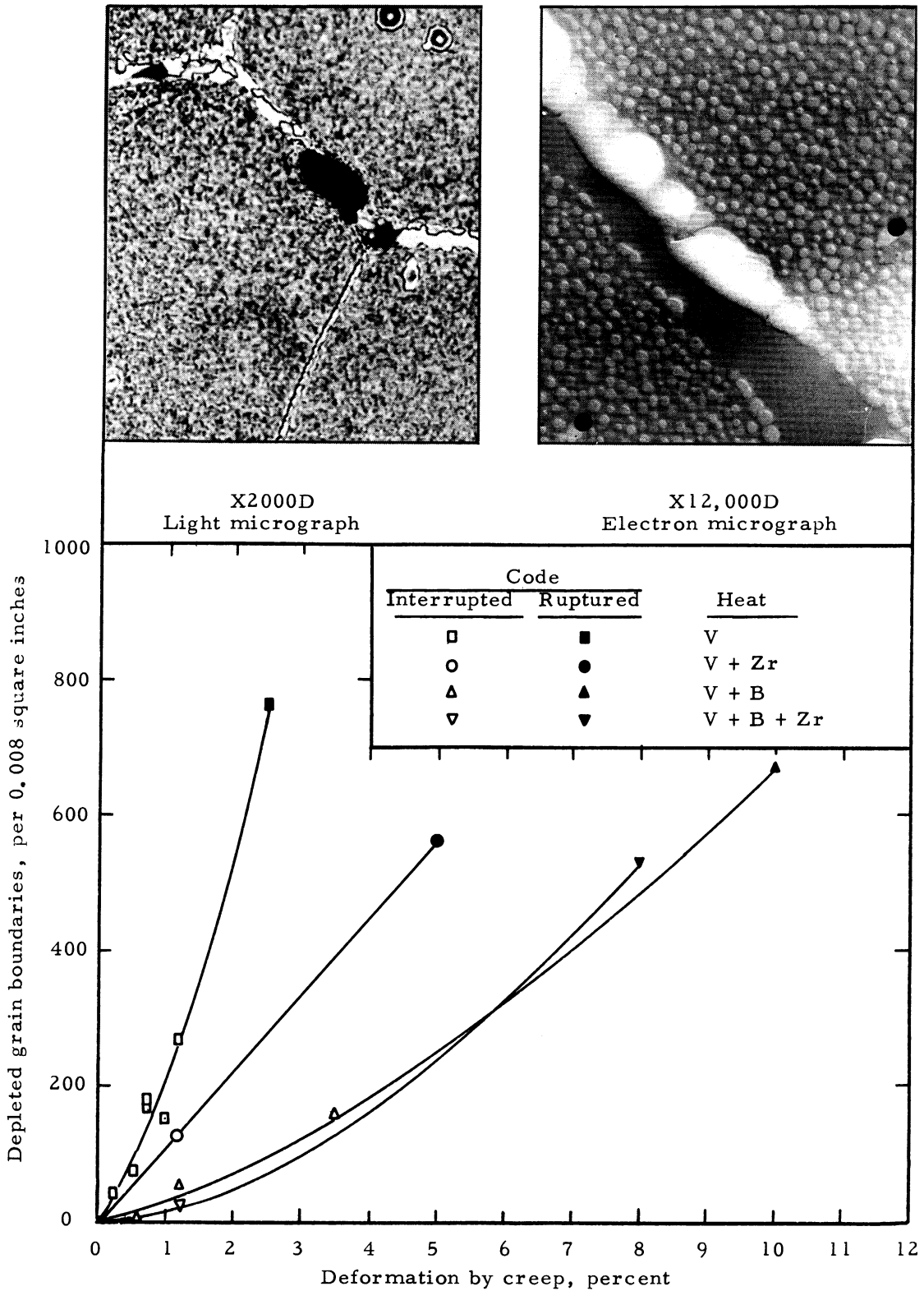
Figure 16. - Effect of creep deformation at 1600°F on depletion of grain boundaries of experimental heats. Stressed to give comparable strain rates. Micrographs of typical depleted grain boundaries are shown for electropolished specimen.
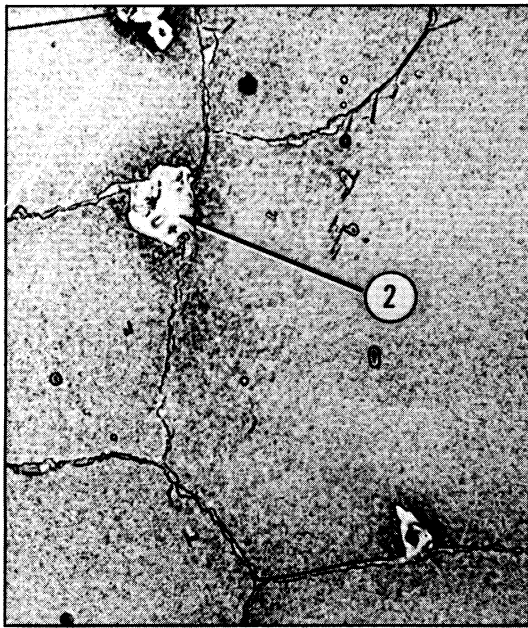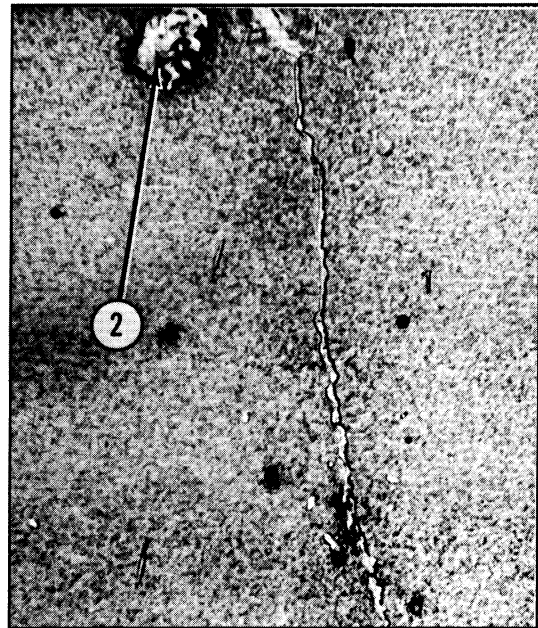
a. Heat V.   DPH-338   b. Heat V + Zr.   DPH-342
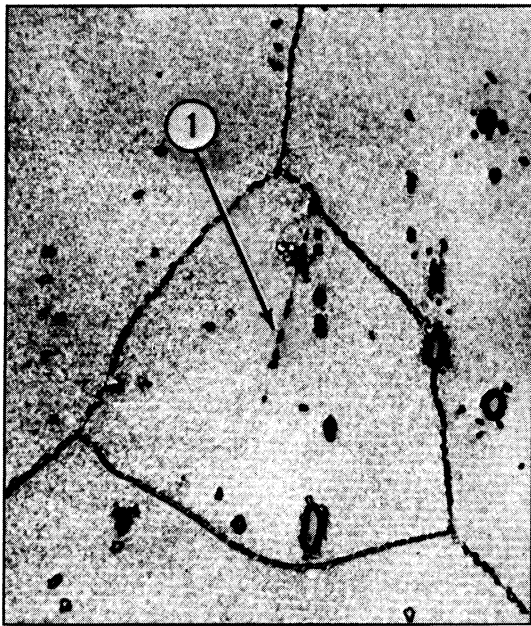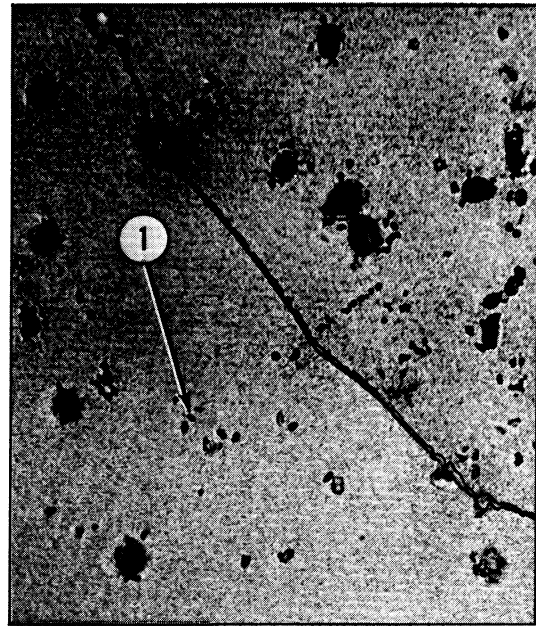
c. Heat V + B.   DPH-340   d. Heat V + B + Zr   DPH-353

Figure 17. -   Microstructures of experimental heats after aging 188 hours
                  at 1600°F. X 1000D. ① - intragranular carbide; ② - nodule.
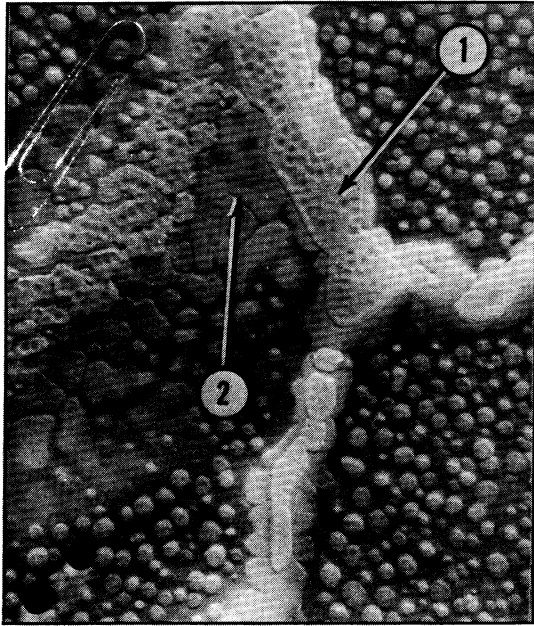
a. Heat V.   b. Heat V + Zr.
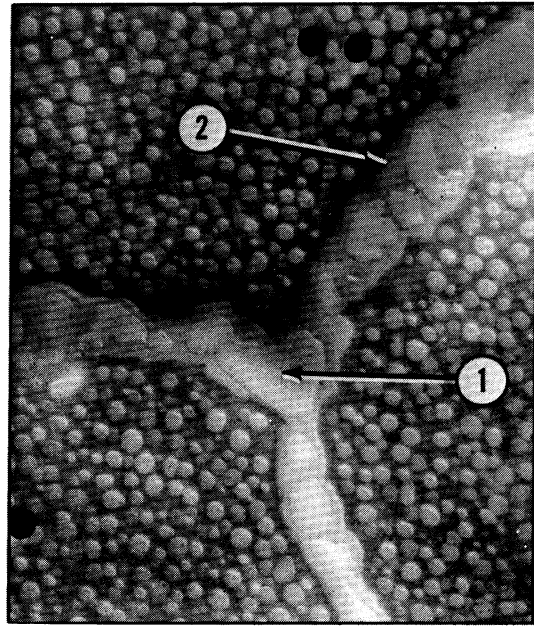
c. Heat V + B.   d. Heat V + B + Zr.

Figure 18. -   Microstructures of experimental heats after aging 188 hours
                  at 1600°F. Electron micrographs X12,000D. ① - inter-
                  granular $M_{23}C_6$; ② - γ'.
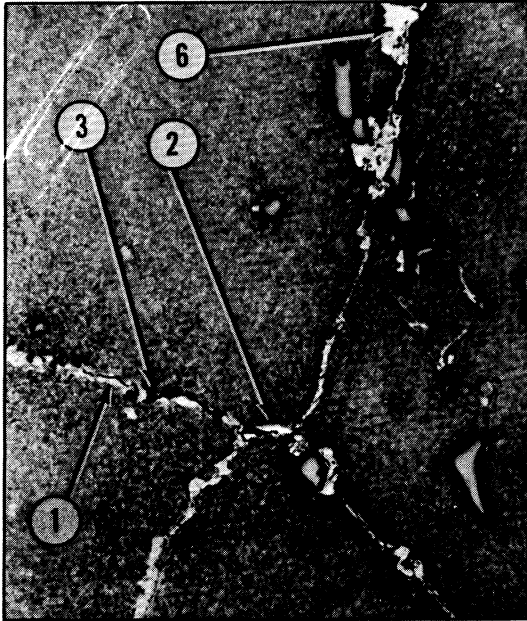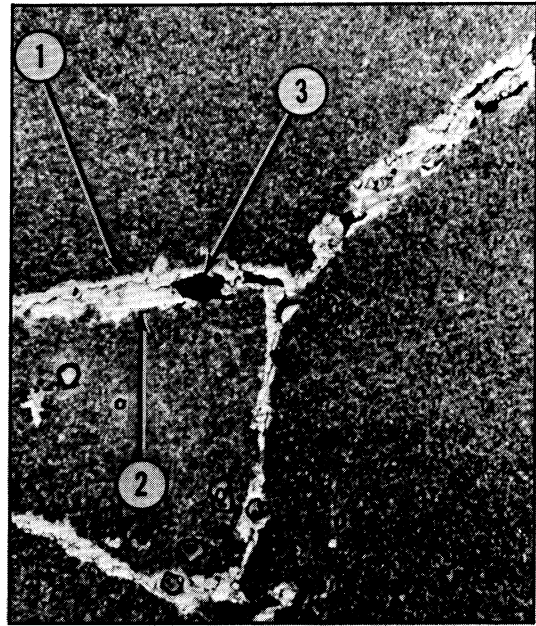
a. Heat V.

b. Heat V + Zr.
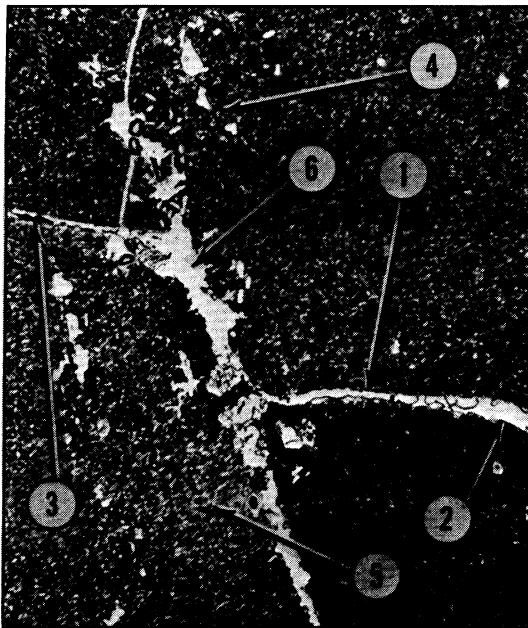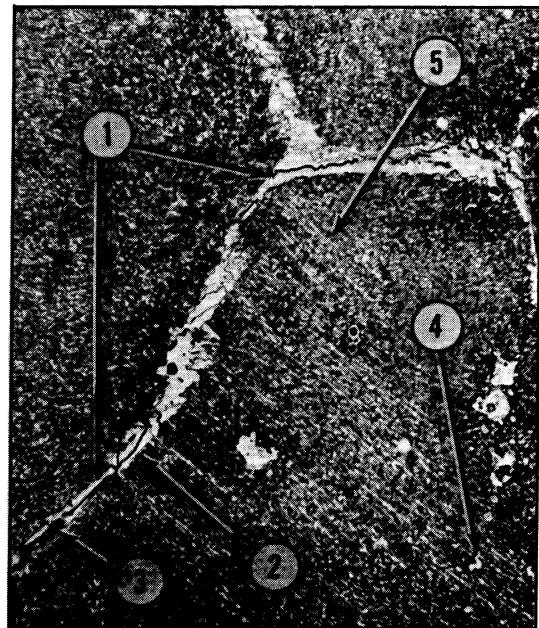
c. Heat V + B.

d. Heat V + B + Zr.

Figure 19. - Microstructures of experimental heats after rupture at 1600°F and 25,000 psi. X1000D. ① - intergranular $M_{23}C_6$; ② - depleted grain boundary; ③ - micro-crack; ④ - intragranular carbide; ⑤ - alignment of γ'; ⑥ - nodule.

X1000D
Light micrograph

X12,000D
Electron micrograph
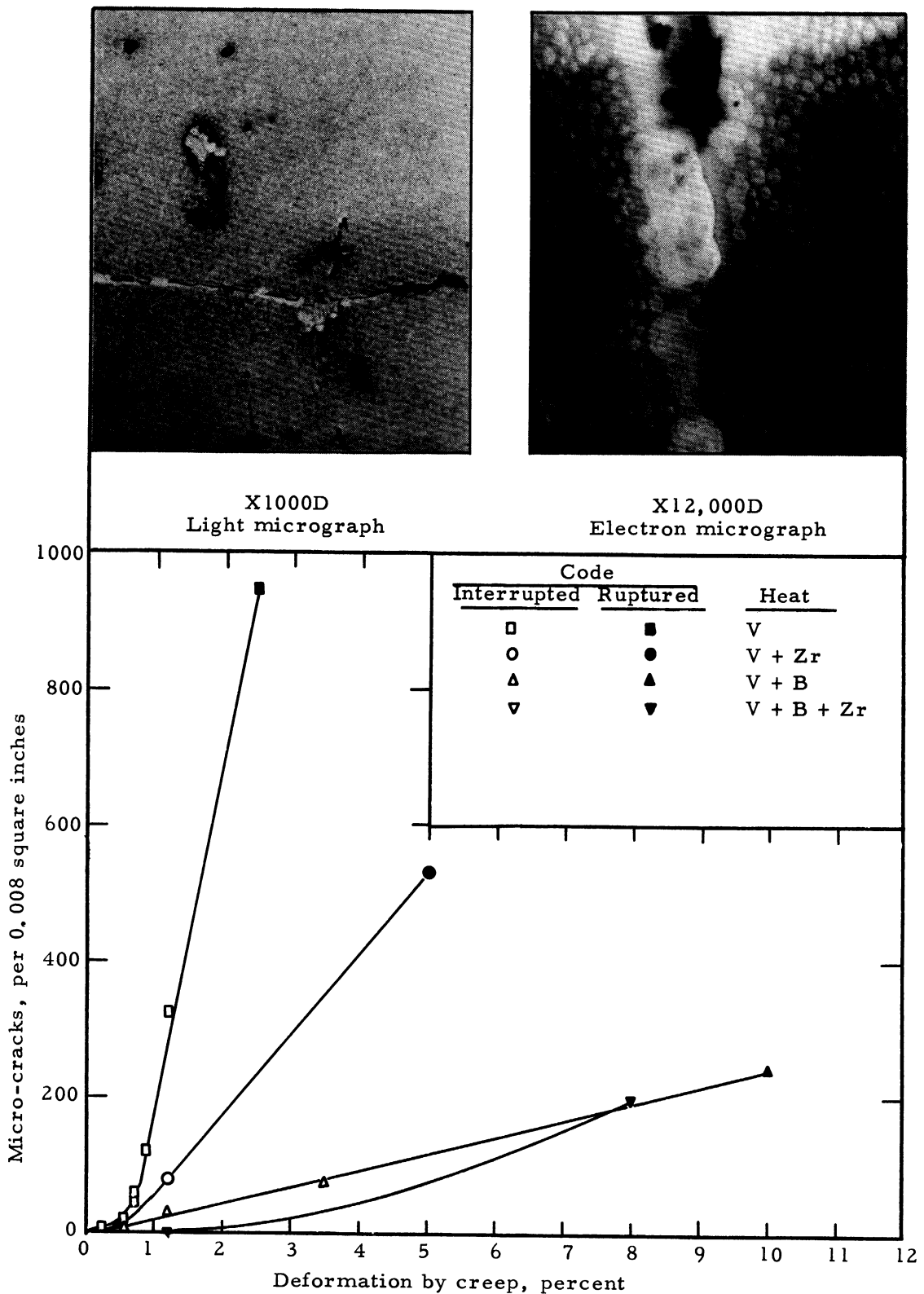
Figure 20. - Effect of creep deformation at 1600°F on micro-cracking of experimental heats. Stressed to give comparable strain rates. Micrographs of typical micro-cracks are shown. Tension axis is horizontal in the electron micrograph.
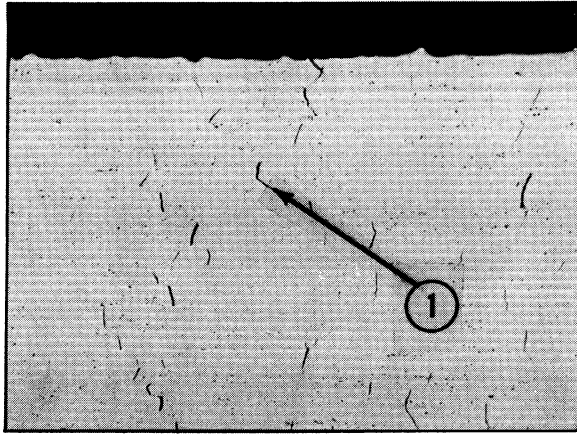
a. Heat V, ruptured in 52 hours at 1600°F and 25,000 psi with 13 surface cracks and 376 micro-cracks.
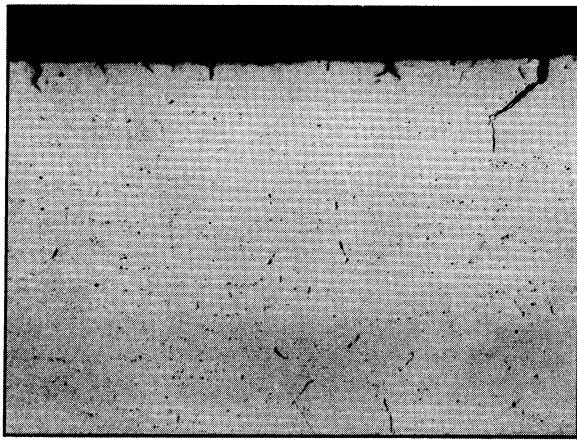
b. Heat V + B, ruptured in 296 hours at 1600°F and 28,000 psi with 160 surface cracks and 243 micro-cracks.
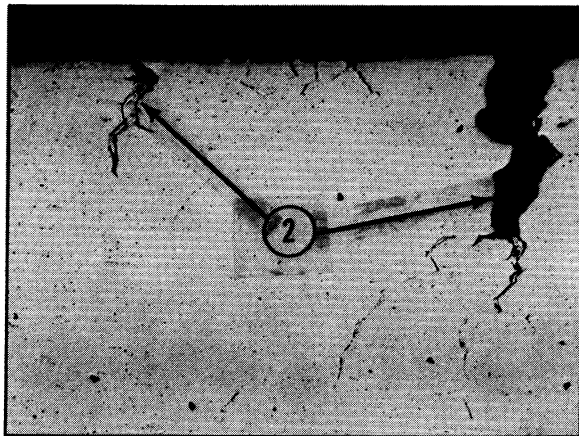
c. Heat V + B + Zr, ruptured in 266 hours at 1600°F and 20,000 psi with 300 surface cracks and 198 micro-cracks.

Figure 21. - Change in mode of cracking in experimental heats. Surface cracks are number per inch of transverse section penetrating more than 0.003 inch. Micro-cracks are number in 0.008 square inches observed. X32D. ① - micro-crack; ② - surface cracks.
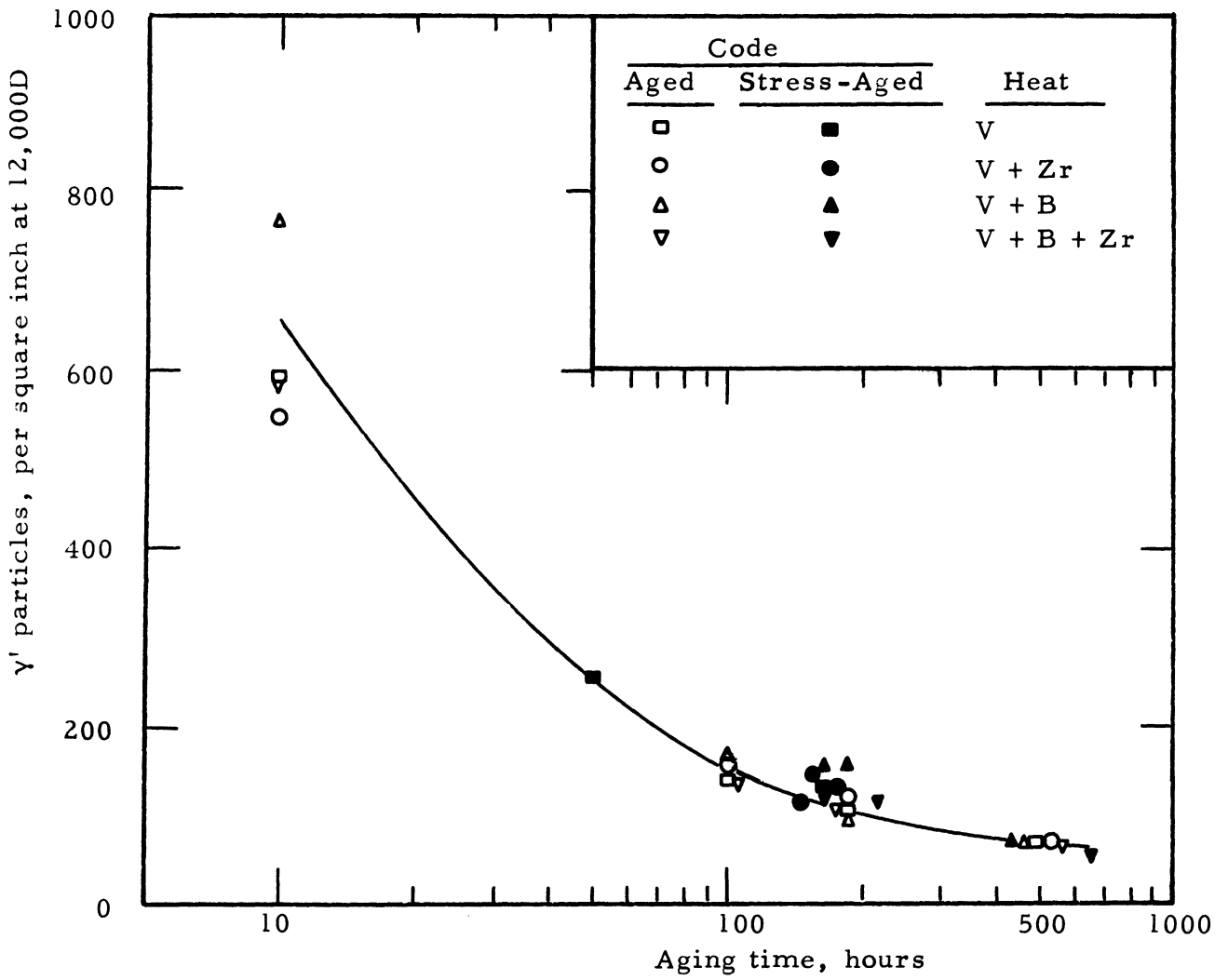
Figure 22. - Effect of aging time at 1600°F on γ' particle density in experimental heats. Stress aging was at 20,000 - 30,000 psi.
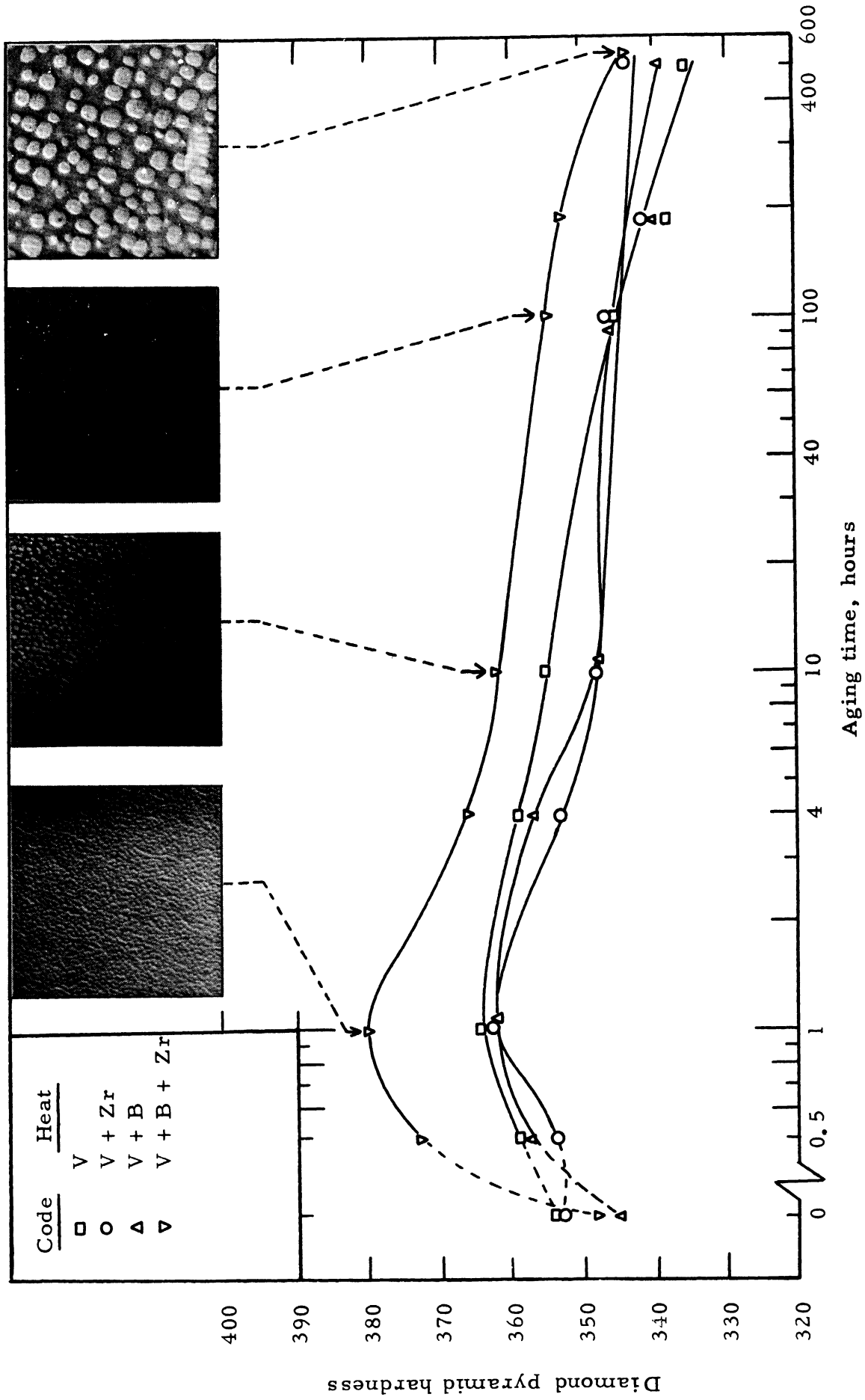
Figure 23. - Effect of aging at 1600°F on hardness and γ' dispersion of experimental heats. Typical electron micrographs at 12,000D are shown.
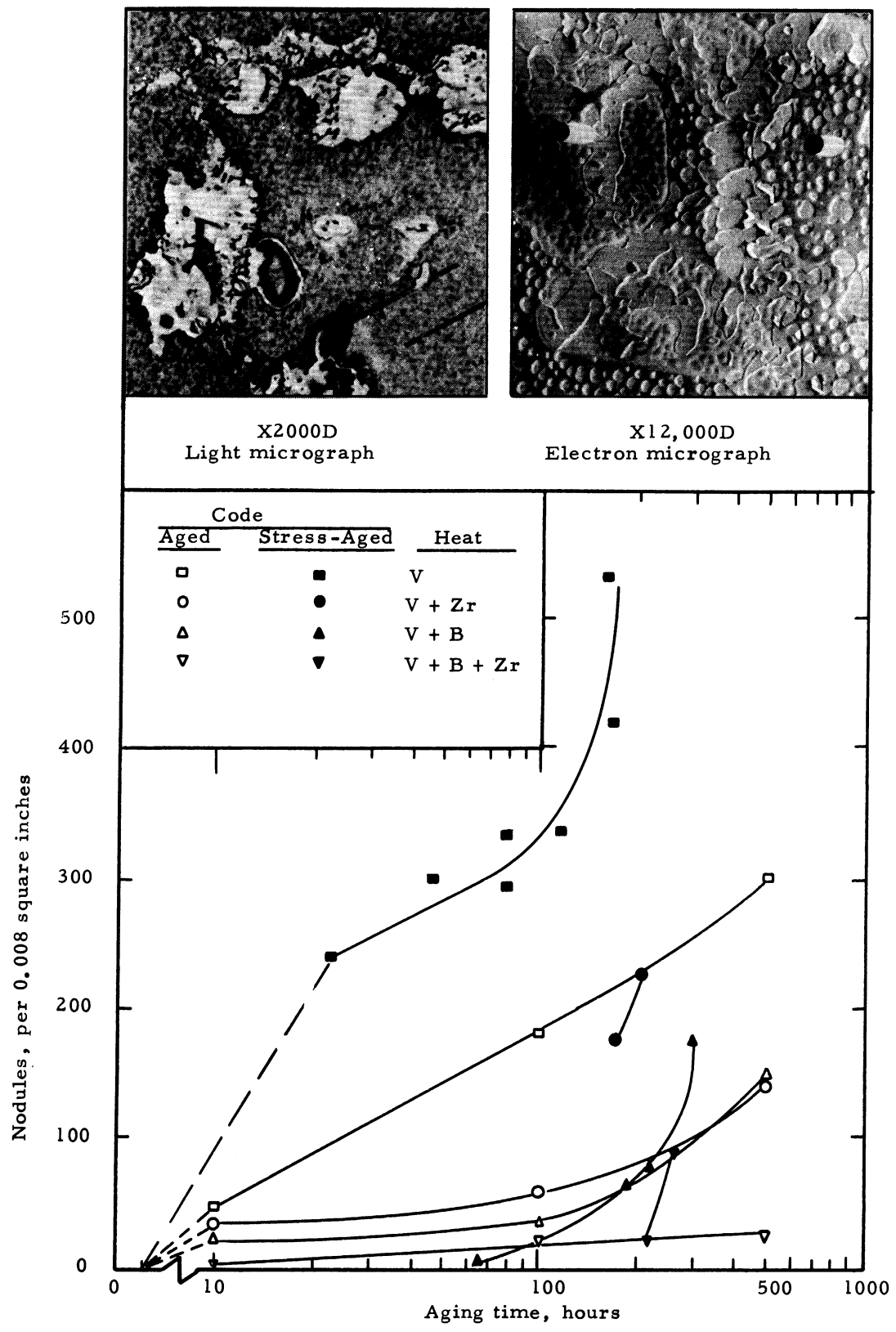
X2000D
Light micrograph

X12,000D
Electron micrograph

Code		
Aged	Stress-Aged	Heat
□	■	V
○	●	V + Zr
△	▲	V + B
▽	▼	V + B + Zr

Nodules, per 0.008 square inches

Aging time, hours

Figure 24. - Effect of aging time at 1600°F on nodule density of experimental heats. Stress aging was at comparable strain rates. Micrographs of typical nodules are shown.
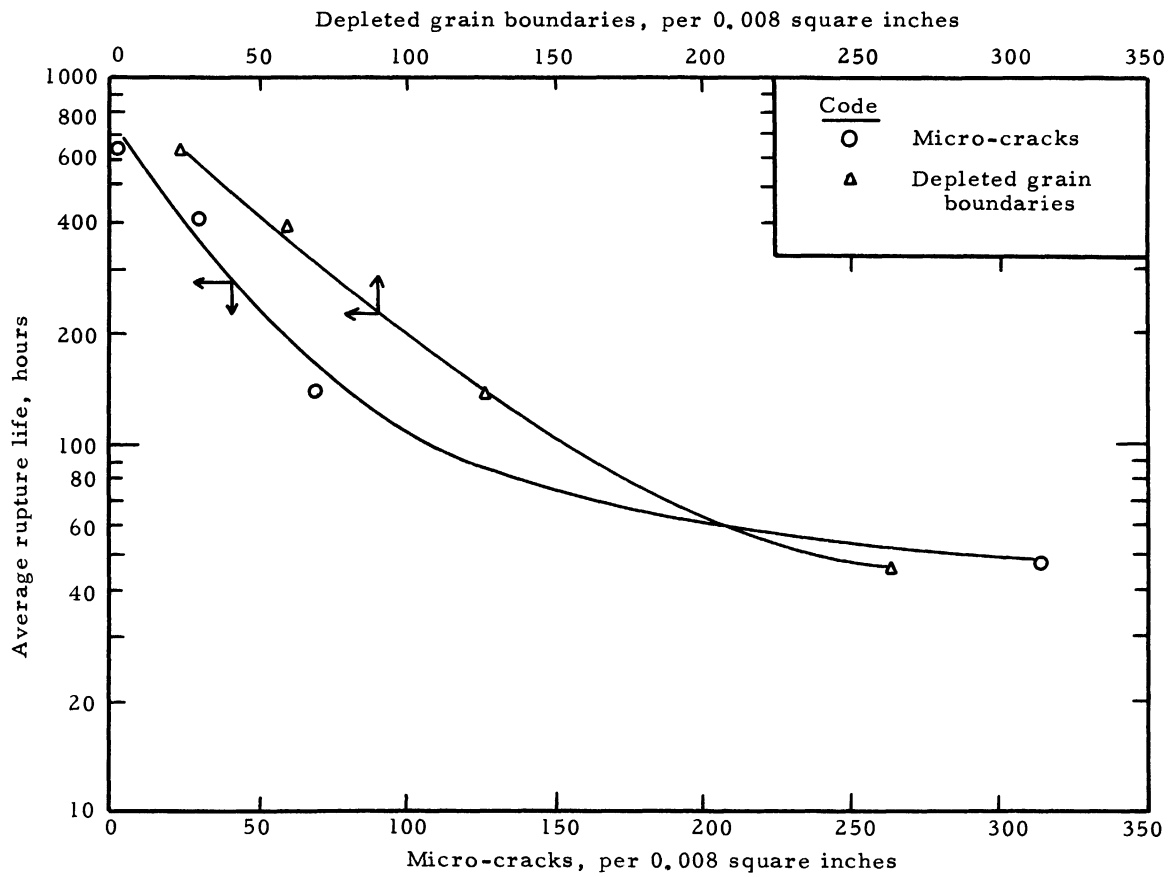
Figure 25. - Relation of rupture life at 1600°F and 25,000 psi to micro-cracking and
depletion tendencies of experimental heats when stressed to give 1.2%
deformation in 165 - 214 hours.

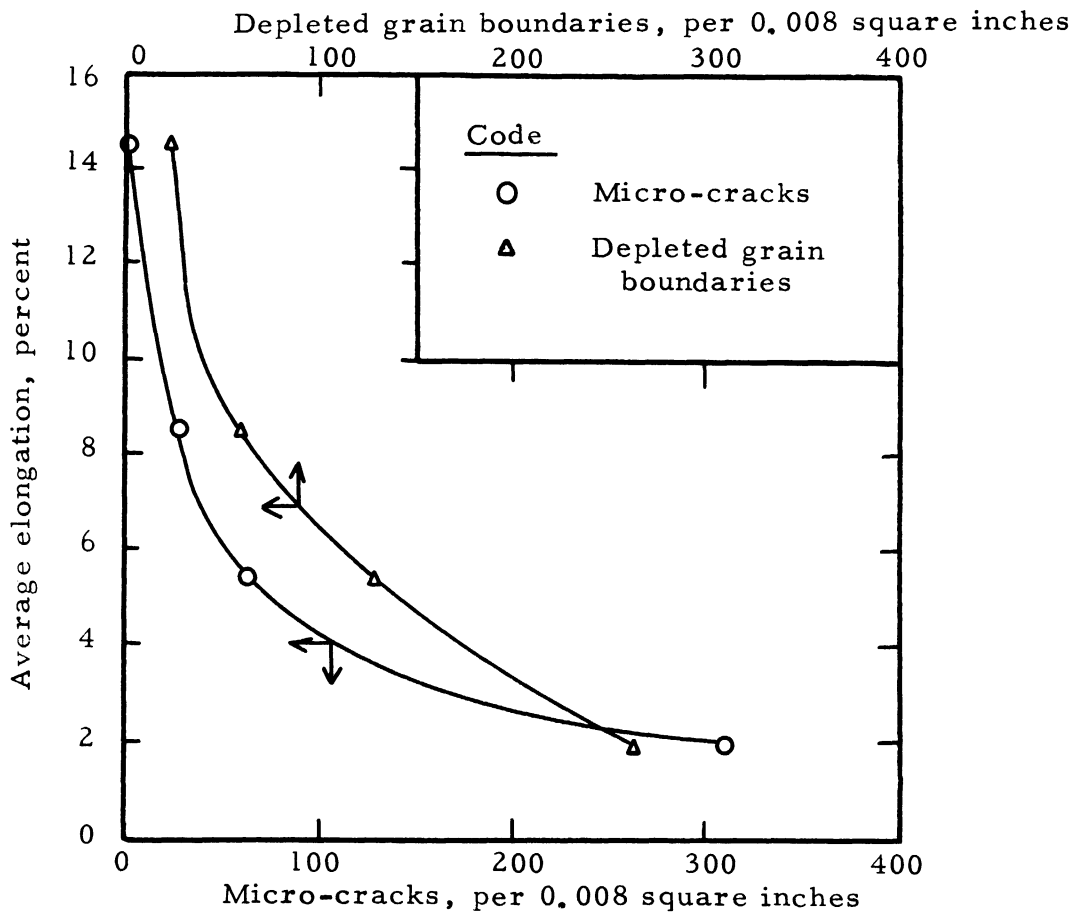Depleted grain boundaries, per 0.008 square inches

Figure 26. - Relation of elongation at 1600°F and
25,000 psi to micro-cracking and
depletion tendencies of experimental
heats when stressed to give 1.2%
deformation in 165-214 hours.